Supplementary data

Flavonoids from *Siparuna cristata* as Potential Inhibitors of SARS-CoV-2 replication

Carla Monteiro Leal[1,2], Suzana Guimarães Leitão*[3], Romain Sausset[2,4], Simony C. Mendonça[2], Pedro H. A. Nascimento[2], Caio Felipe de Araujo R. Cheohen[5], Maria Eduarda A. Esteves[6], Manuela Leal da Silva[5,6], Tayssa Santos Gondim[7], Maria Eduarda S. Monteiro[7], Amanda Resende Tucci[7], Natália Fintelman-Rodrigues[8,9], Marilda M. Siqueira[7], Milene Dias Miranda[7], Fernanda N. Costa[2], Rosineide C. Simas[10], Gilda Guimarães Leitão*[2]

[1]Programa de Pós-graduação em Biotecnologia Vegetal e Bioprocessos, Universidade Federal do Rio de Janeiro, Rio de Janeiro, RJ, Brazil, 21.941-902.

[2]Instituto de Pesquisas de Produtos Naturais, Universidade Federal do Rio de Janeiro, Centro de Ciências da Saúde, Bl. H, Ilha do Fundão, Rio de Janeiro, RJ, Brazil, 21.941-902.

[3]Faculdade de Farmácia, Universidade Federal do Rio de Janeiro, Centro de Ciências da Saúde, Bl. A 2º andar, Ilha do Fundão, Rio de Janeiro, RJ, Brazil, 21.941-902.

[4]Muséum National d'Histoire Naturelle, Paris, France, 75005.

[5]Programa de Pós-graduação Multicêntrico em Ciências Fisiológicas, Universidade Federal do Rio de Janeiro, Centro de Ciências da Saúde, Instituto de Biodiversidade e Sustentabilidade NUPEM, Macaé, RJ, 27.965-045, Brazil.

[6]Programa de Pós-graduação em Biologia Computacional e Sistemas, Instituto Oswaldo Cruz, Manguinhos, Rio de Janeiro, RJ, Brazil, 21.041-361.

[7]Laboratório de Vírus Respiratórios e do Sarampo, Instituto Oswaldo Cruz, Fundação Oswaldo Cruz, Rio de Janeiro, 21.041-210, Brazil

[8]Laboratório de Imunofarmacologia, Instituto Oswaldo Cruz, Fundação Oswaldo Cruz, Rio de Janeiro, 21.041-210, Brazil

[9]Instituto Nacional de Ciência e Tecnologia de Gestão da Inovação em Doenças Negligenciadas, Centro de Desenvolvimento Tecnológico em Saúde, Fundação Oswaldo Cruz, Rio de Janeiro, RJ, 21.041-210, Brazil

[10]Laboratório de Cromatografia e Espectrometria de Massas, Instituto de Química, Universidade Federal de Goiás, Goiânia, GO, Brazil, 74.690-900.

* Corresponding authors:
Suzana Guimarães Leitão
Email address: sgleitao@pharma.ufrj.br; sgleitao@gmail.com

Gilda Guimarães Leitão
E-mail address: ggleitao@ippn.ufrj.br

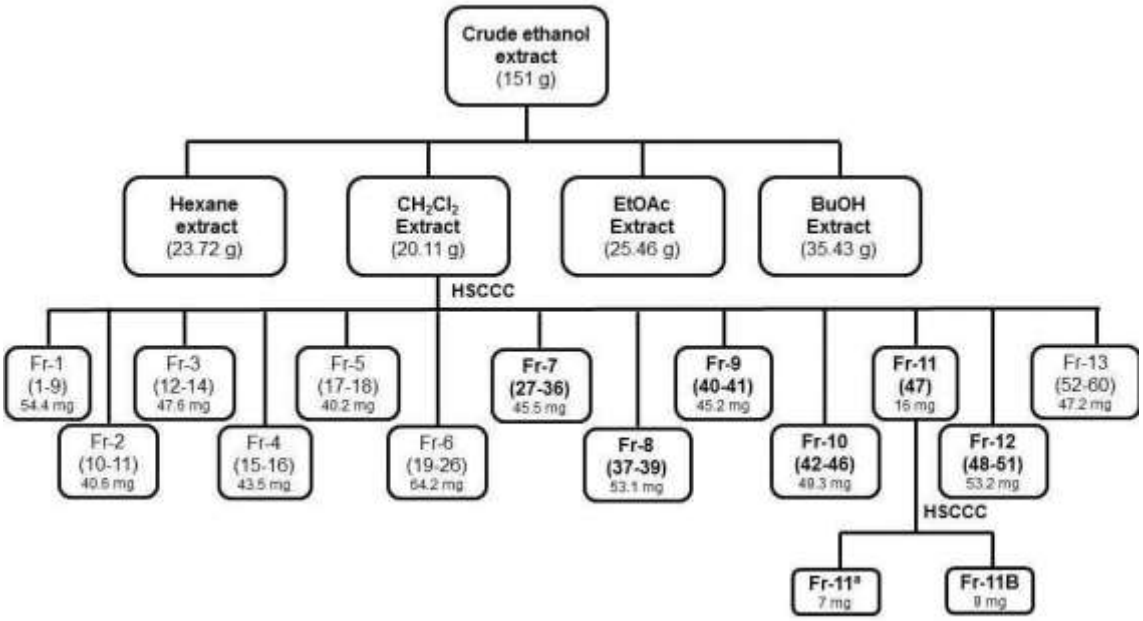

Fig. S1 Flowchart of the fractionation of the crude ethanol extract of *S. cristata* leaves.

Detailed description of of fractions Fr-7 to Fr-12 annotations

The HPLC-DAD chromatogram of fractions Fr-7 to Fr-12 showed only two different ultraviolet profiles compatible with kaempferol and quercetin derivatives (Fig. S2 to S7), a common feature in *Siparuna* genus. Flavonoids with these two aglycones have been previously isolated from *S. apiosyce* (Leitão et al. 2000), *S. guianensis* (Leitão et al. 2005), *S. glycycarpa* (Costa et al. 2013) and *S. gigantotepala*. Kaempferol and quercetin display two absorption maxima in the ultraviolet-visible for Bands I and II, in the ranges 300-380 nm and 240-285 nm, respectively, which is in accordance with our data, suggesting the presence of three major derivatives of quercetin in peaks at *Rt* 29.4, 32.7 and 36.7min; as well as one kaempferol derivative at *Rt* 32.2 min.

The positive mode APCI ionization source was chosen for the MS analyzes (Table S1 and Fig. S8 to S19) of the fractions. The profile showed three major compounds with intense protonated molecular ions $[M + H]^+$, in the range of *m/z* 100 to 1000, so three major masses were detected: i) DI-APCI-MS/MS for compound **1** (obtained from Fr-7**,** *Rt* 29.4 min, Fig. S8 to S9) displayed fragments at *m/z* 330 $[M + H - CH_3]^+$ and 315 $[M + H - 2\times CH_3]^+$ corresponding to the neutral losses of two

methyl groups. The molecular mass obtained was 345 $[M + H]^+$, compatible with the molecular formula $C_{18}H_{16}O_7$, and the compound was identified as tri-*O*-methyl-quercetin (**1**) by comparison with ^1H, ^{13}C and 2D NMR (Fig. S20 to S27). Compound **1** was therefore identified as 3,3',4'-tri-*O*-methyl-quercetin (Table S1) (Awad et al. 2018). As far as we know, the ^{13}C NMR data for this compound, isolated for the first time from *Ericameria diffusa* is being reported here for the first time (Urbatsch et al. 1976); ii) Fr-10 consisted of compound **3** (*Rt* 32.2 min), showing $[M + H]^+$ at *m/z* 315, with its CID MS spectra contain peaks at *m/z* 300 $[M + H - CH_3]^+$ and 287 $[aglycone + H]^+$ compatible with di-*O*-methyl-kaempferol structure, $C_{17}H_{14}O_6$ (Fig. S14 to S15). The structure of 3,7-di-*O*-methyl-kaempferol or kumatakenin (**3**) was confirmed by NMR analyses and is in accordance with those reported in the literature (Fig. S30 to S37, Table S2) (Silva et al. 2009). This compound was also isolated from Fr-11 (Fig. S16 to S17; Fig. S38 to S40) by further purification by HSCCC (fraction 11B; Fig. S45 to S50), which also afforded tetra-*O*-methyl-quercetin or retusin (**2)** (*Rt* 36.7 min, $[M + H]^+$ 359), in fraction 11A (Fig. S41 to S44); and ii) The analysis of fraction 11A by NMR showed in the ^1H spectrum signals of methoxyl groups with integration for 4 MeO (Fig. S44) and aromatic protons from the AB and ABC systems (Fig. S42 to S43) corresponding to tetra-*O*-methyl-quercetin. The signal at δ_H 12.65 (Fig. S41) confirmed the presence of the free 5-OH group in a hydrogen bond with C-4 carbonyl, confirming the presence of 3,7,3',4'-tetra-*O*-methyl-quercetin (retusin) (**2**) (Silva et al. 2009) in this fraction.

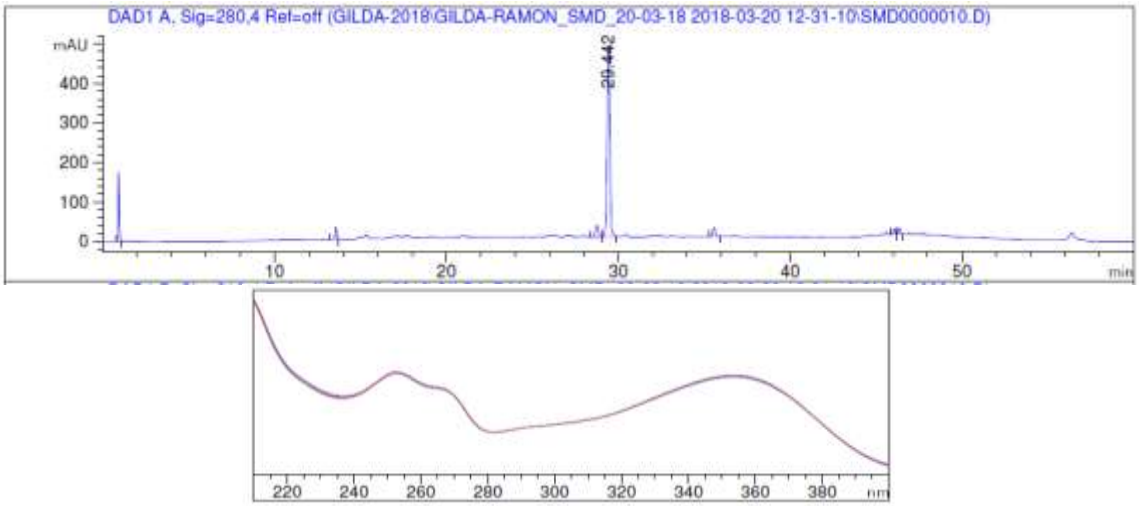

Fig. S2 HPLC-DAD profile of Fr-7 and UV spectrum of peak at 29.4 min at 280nm (3,3',4'-tri-*O*-methyl-quercetin, **1**).

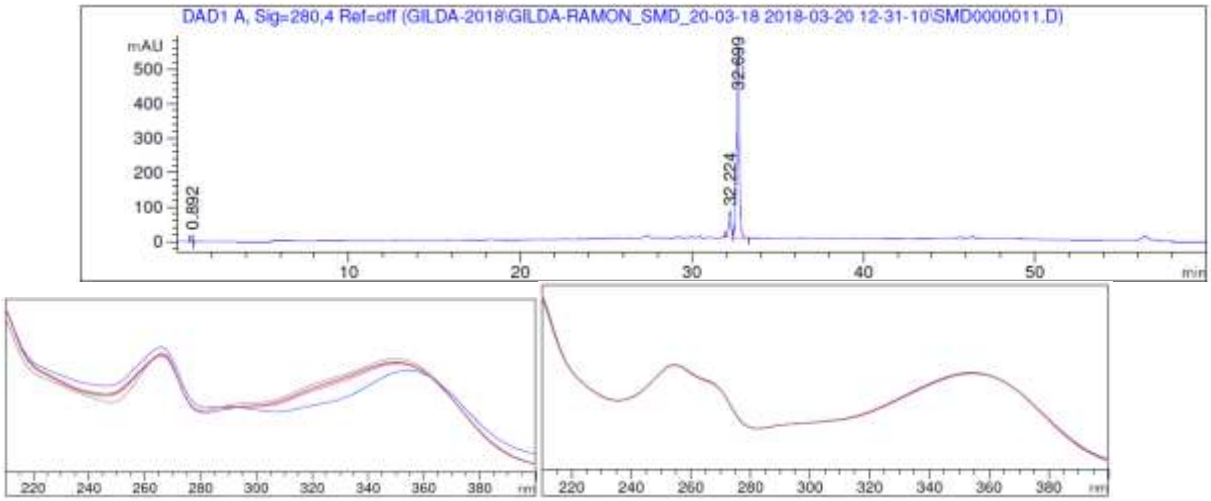

Fig. S3 HPLC-DAD profile of Fr-8 and UV spectra of peaks at 32.2 and 32.7 min at 280nm (di-*O*-methyl-kaempferol and tri-*O*-methyl-quercetin).

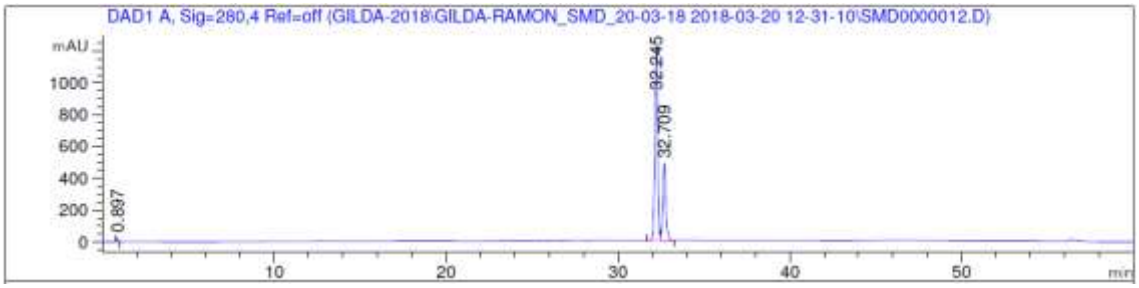

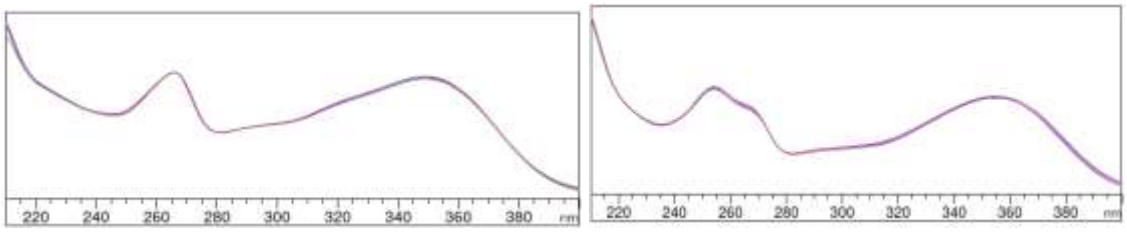

Fig. S4 HPLC-DAD profile of Fr-9 and UV spectra of peaks at 32.2 and 32.7 min at 280nm (di-*O*-methyl-kaempferol and tri-*O*-methyl-quercetin).

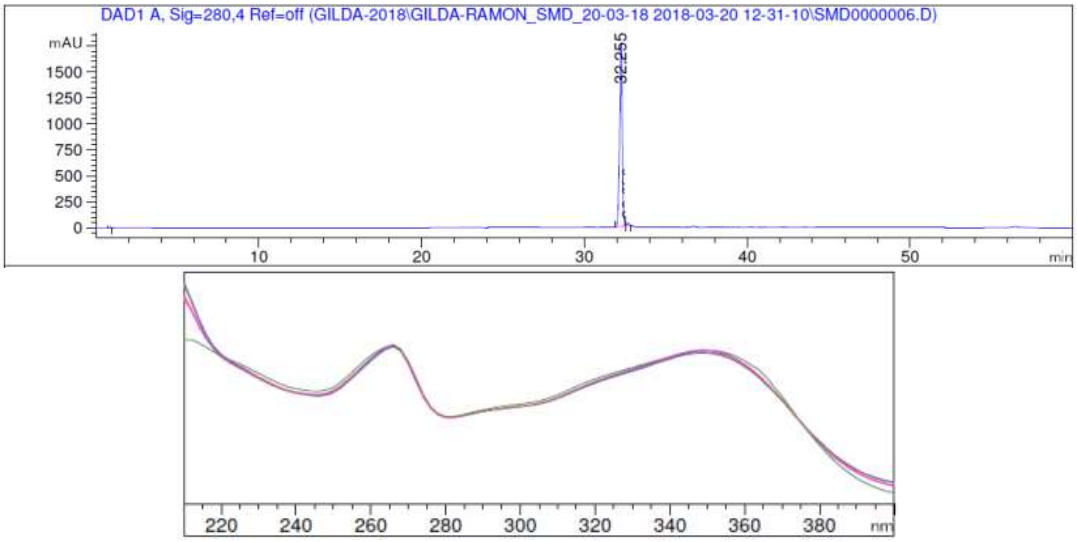

Fig. S5 HPLC-DAD profile of Fr-10 and UV spectrum of peak at 32.2 min at 280nm (di-*O*-methyl-kaempferol (kumatakenin), **3**).

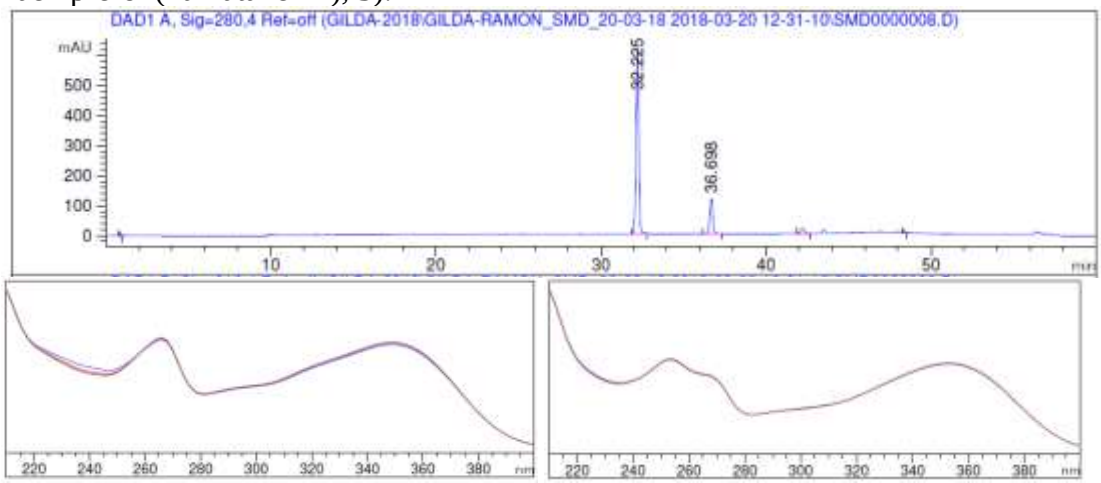

Fig. S6 HPLC-DAD profile of Fr-11 and UV spectra of peaks at 32.2 and 36.7 min at 280nm (3,7-di-*O*-methyl-kaempferol (kumatakenin), **3** and tetra-*O*-methyl-quercetin (retusin), **2**).

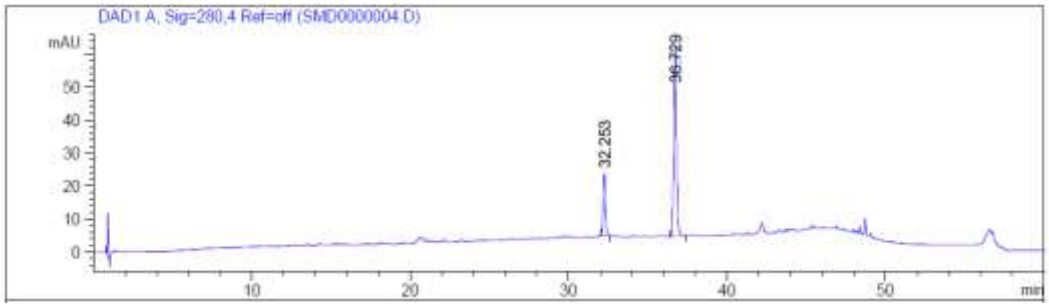

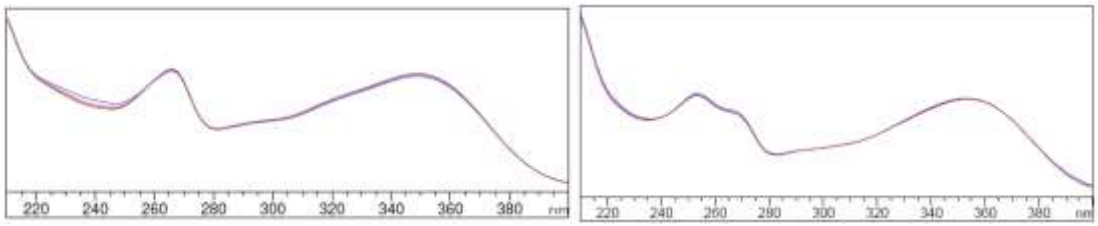

Fig. S7 HPLC-DAD profile of Fr-12 and UV spectra of peaks at 32.2 and 36.7 min at 280nm (3,7-di-*O*-methyl-kaempferol (kumatakenin), **3** and tetra-*O*-methyl-quercetin (retusin), **2**).

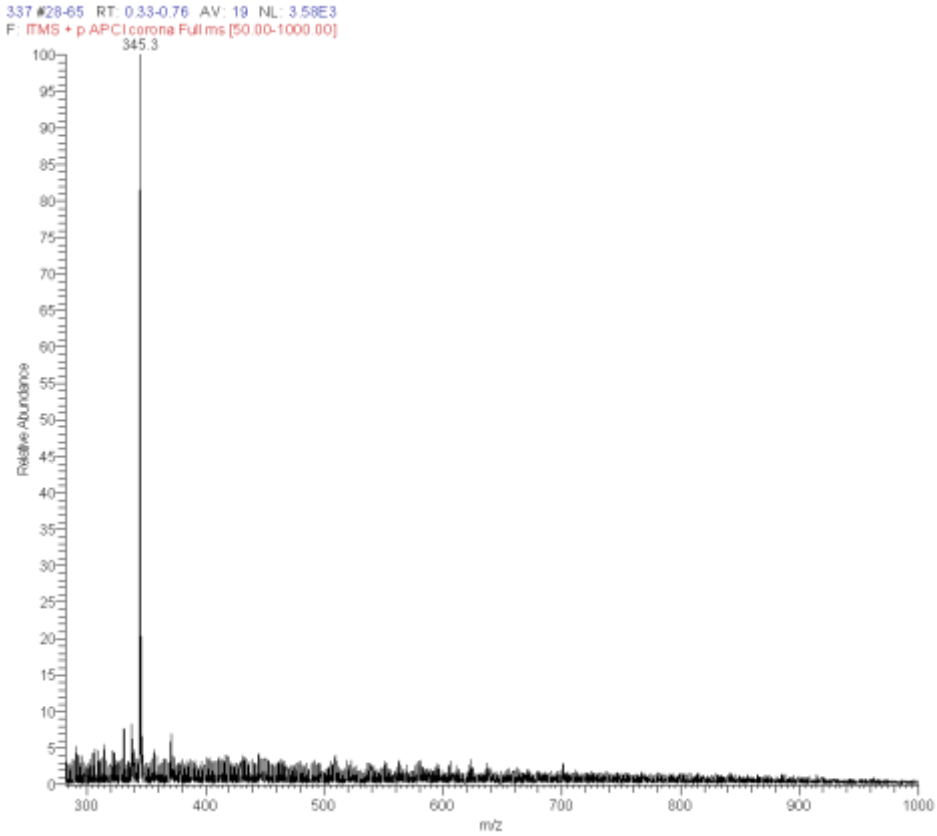

Fig. S8 MS profile of **Fr-7** (R_t = 29.4 min; (3,3',4'-tri-*O*-methyl-quercetin, **1**).

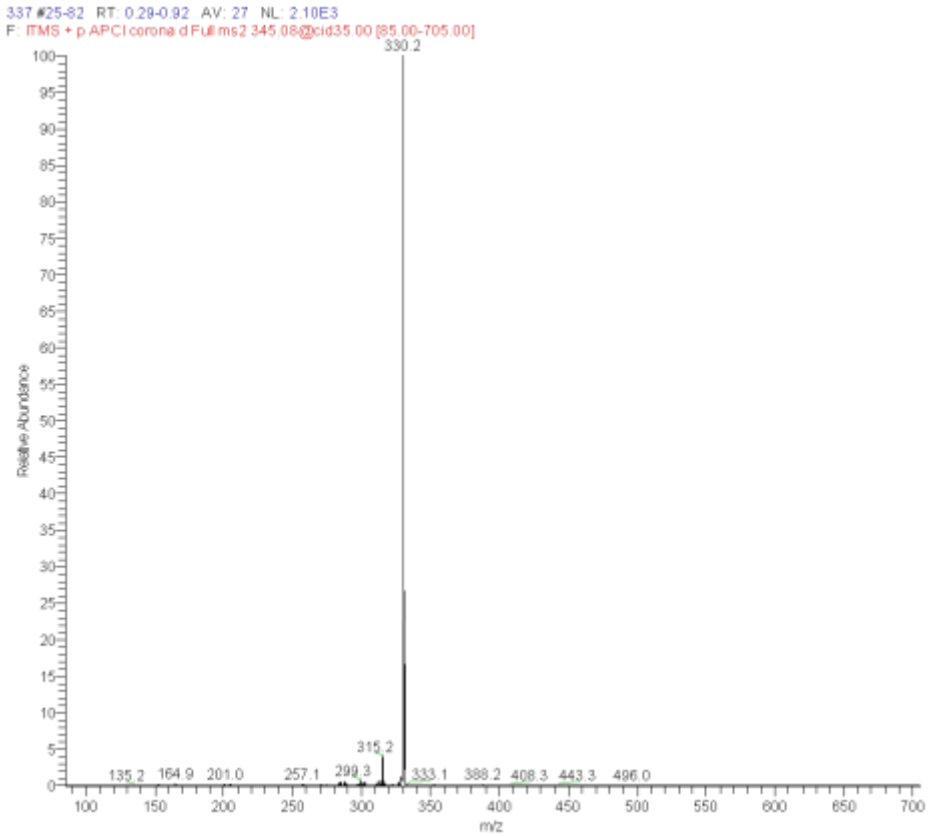

Fig. S9 Product ion spectrum obtained by CID (35eV) of the precursor ion *m/z* 345 in **Fr-7** produced by APCI ionization of 3,3',4'-tri-*O*-methyl-quercetin, **1**.

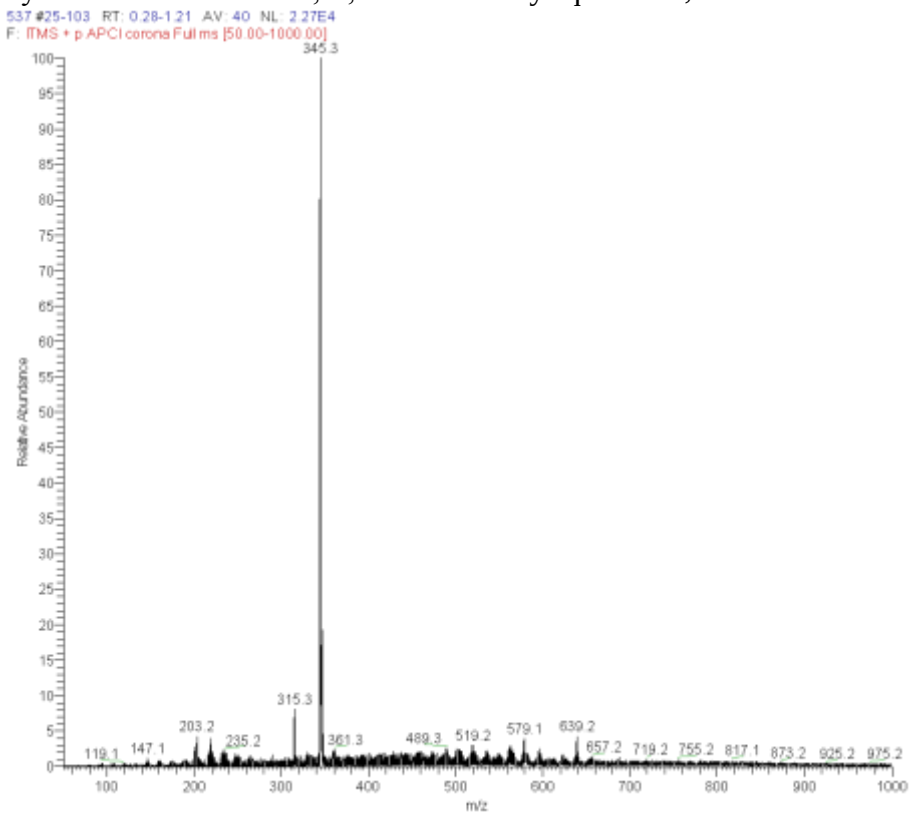

Fig. S10 MS profile of **Fr-8** (R_t= 32.2 min; di-*O*-methyl-kaempferol and R_t= 32.7 min; tri-*O*-methyl-quercetin).

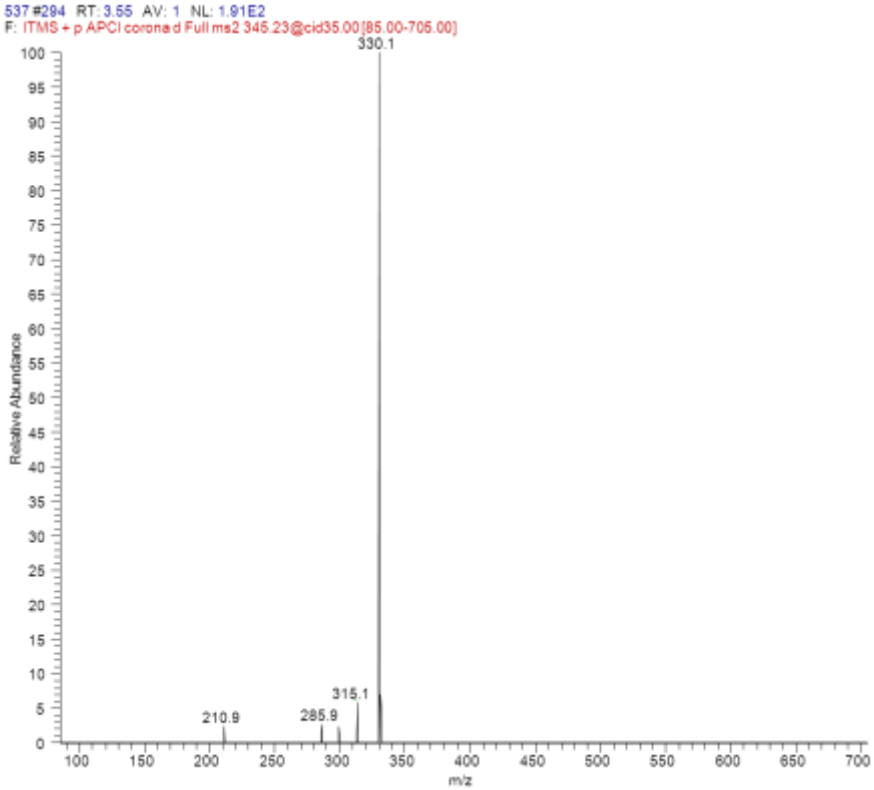

Fig. S11 Product ion spectrum obtained by CID (35eV) of the precursor ion *m/z* 345 in **Fr-8** produced by APCI ionization of tri-*O*-methyl-quercetin.

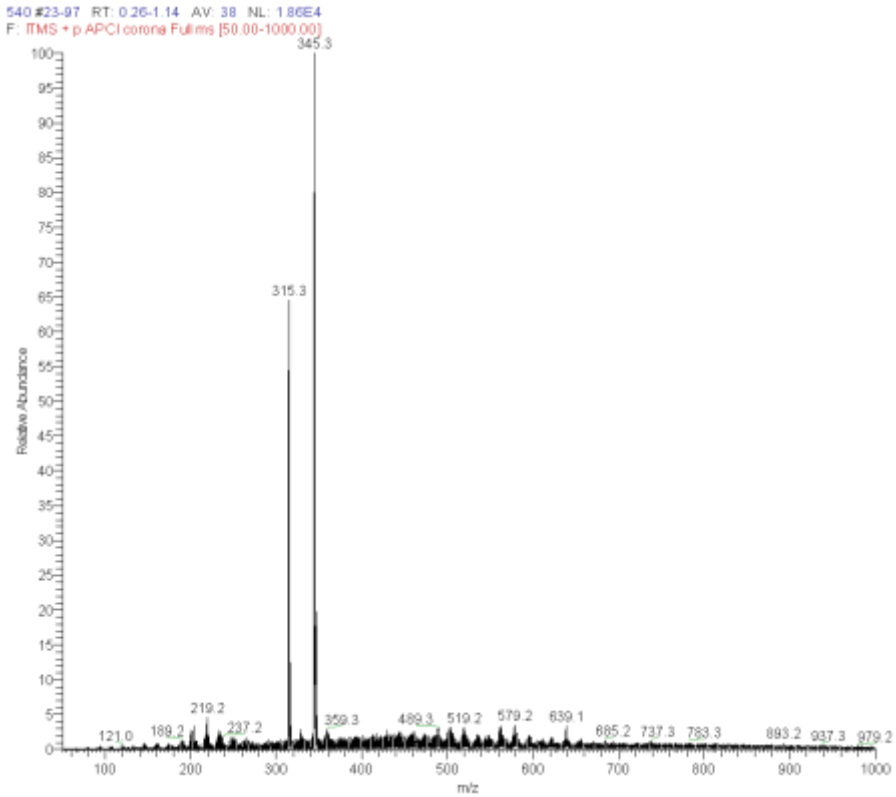

Fig. S12 MS profile of **Fr-9** (R_t = 32.2 min; di-*O*-methyl-kaempferol and R_t = 32.7 min; tri-*O*-methyl-quercetin).

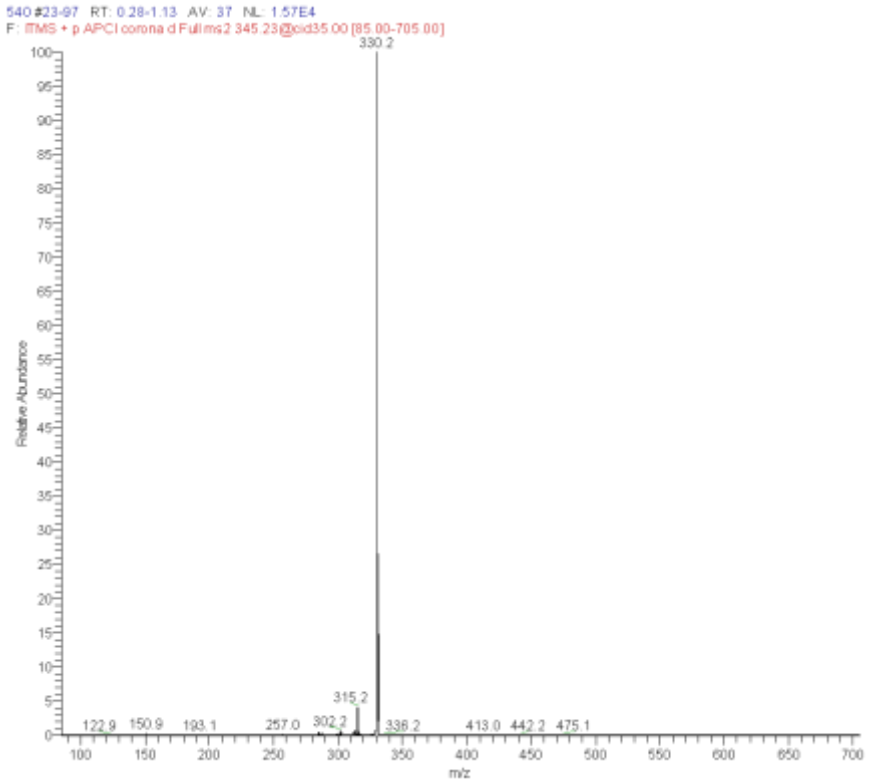

Fig. S13 Product ion spectrum obtained by CID (35eV) of the precursor ion *m/z* 345 in **Fr-9** produced by APCI ionization of tri-*O*-methyl-quercetin.

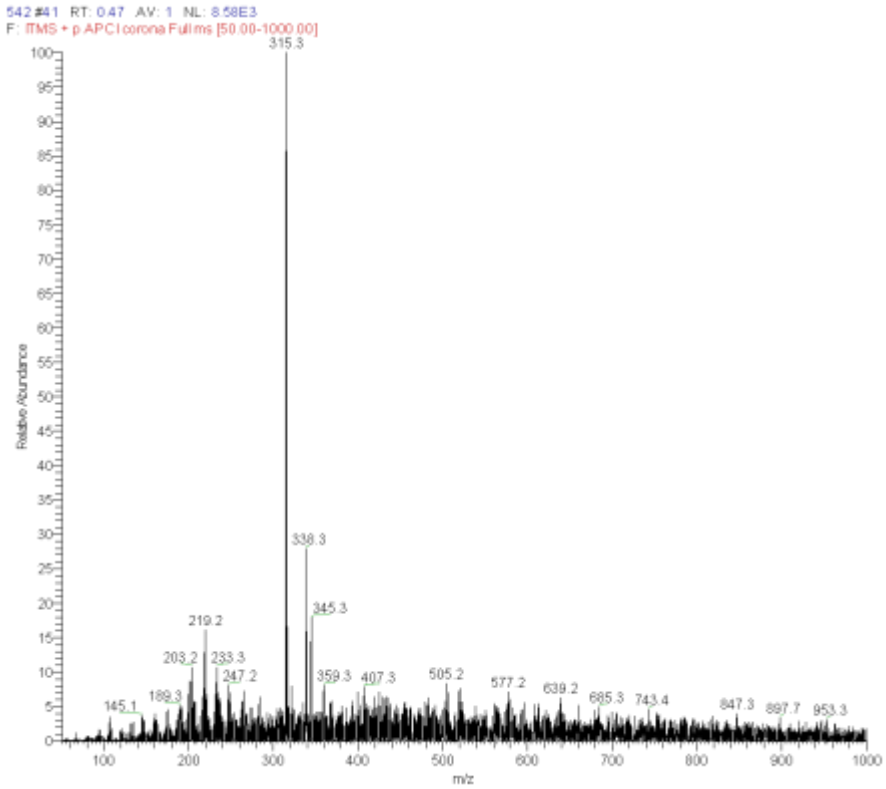

Fig. S14 MS profile of **Fr-10** (R_t = 32.2 min; 3,7-di-*O*-methyl-kaempferol (kumatakenin), **3**).

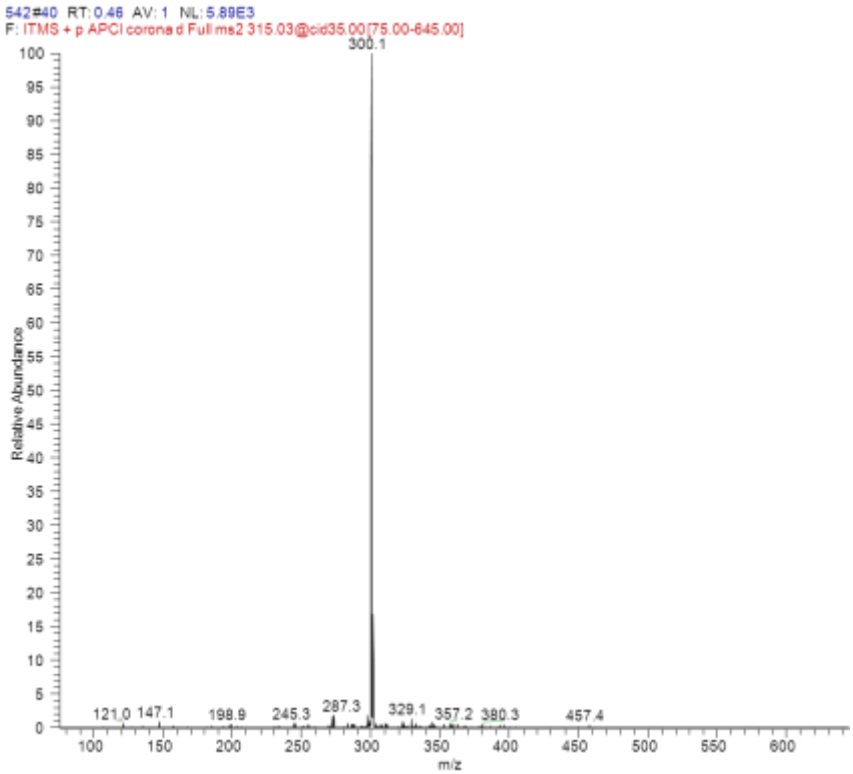

Fig. S15 Product ion spectrum obtained by CID (35eV) of the precursor ion *m/z* 315 in **Fr-10** produced by APCI ionization of 3,7-di-*O*-methyl-kaempferol (kumatakenin), **3**).

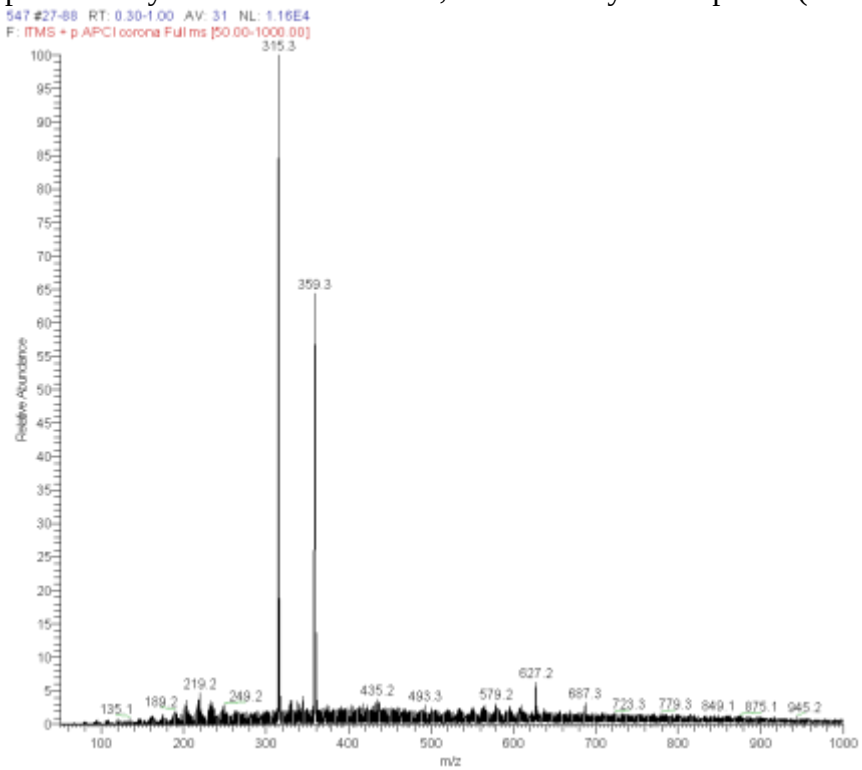

Fig. S16 MS profile of **Fr-11** (R_t = 32.2 min; 3,7-di-*O*-methyl-kaempferol (kumatakenin), **3** and R_t = 36.7 min; tetra-*O*-methyl-quercetin (retusin), **2**).

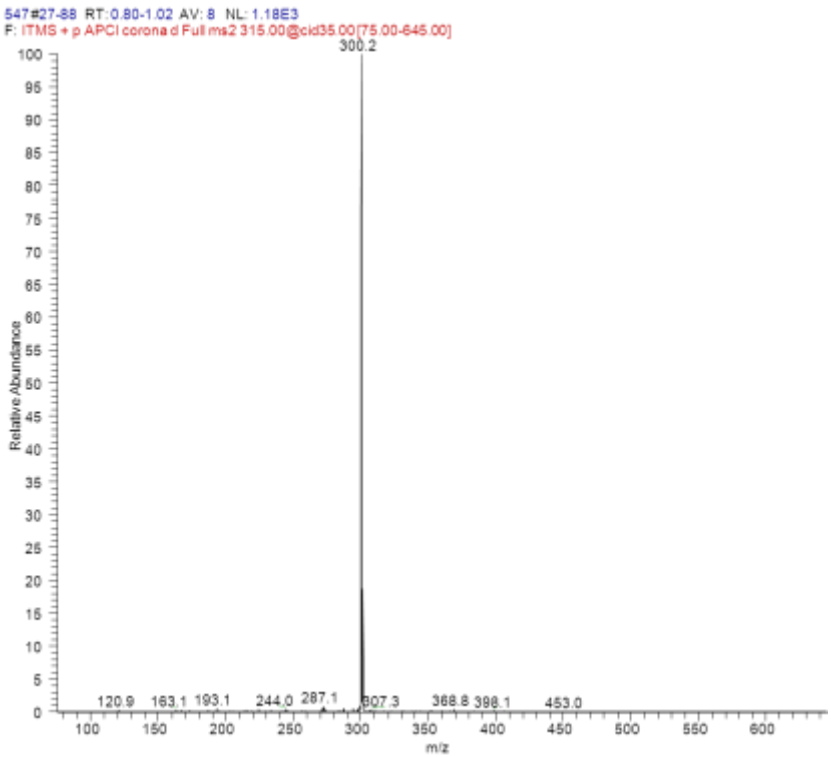

Fig. S17 Product ion spectrum obtained by CID (35eV) of the precursor ion *m/z* 315 in **Fr-11** produced by APCI ionization of di-*O*-methyl-kaempferol.

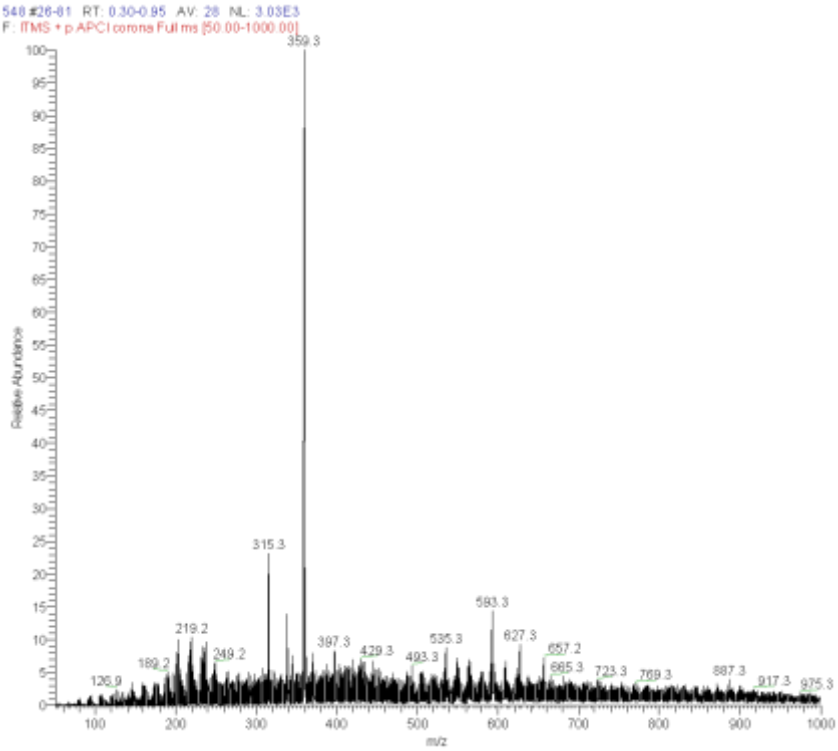

Fig. S18 MS profile of **Fr-12** (R_t = 32.2 min; di-*O*-methyl-kaempferol and R_t = 36.7 min; tetra-*O*-methyl-quercetin (retusin), **2**).

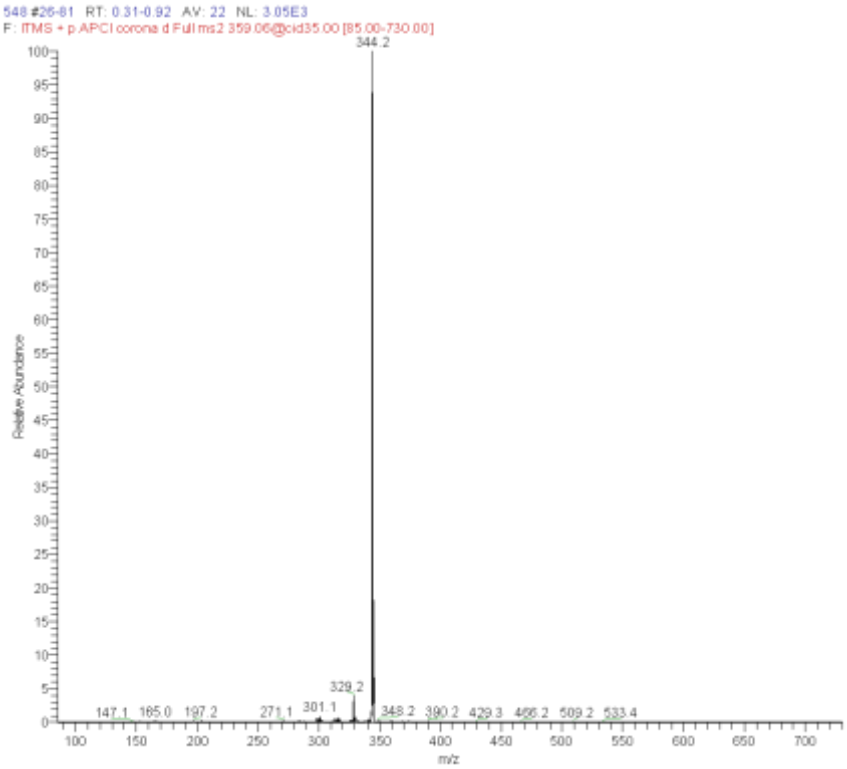

Fig. S19 Product ion spectrum obtained by CID (35eV) of the precursor ion *m/z* 359 in **Fr-12** produced by APCI ionization of tetra-*O*-methyl-quercetin (retusin), **2**.

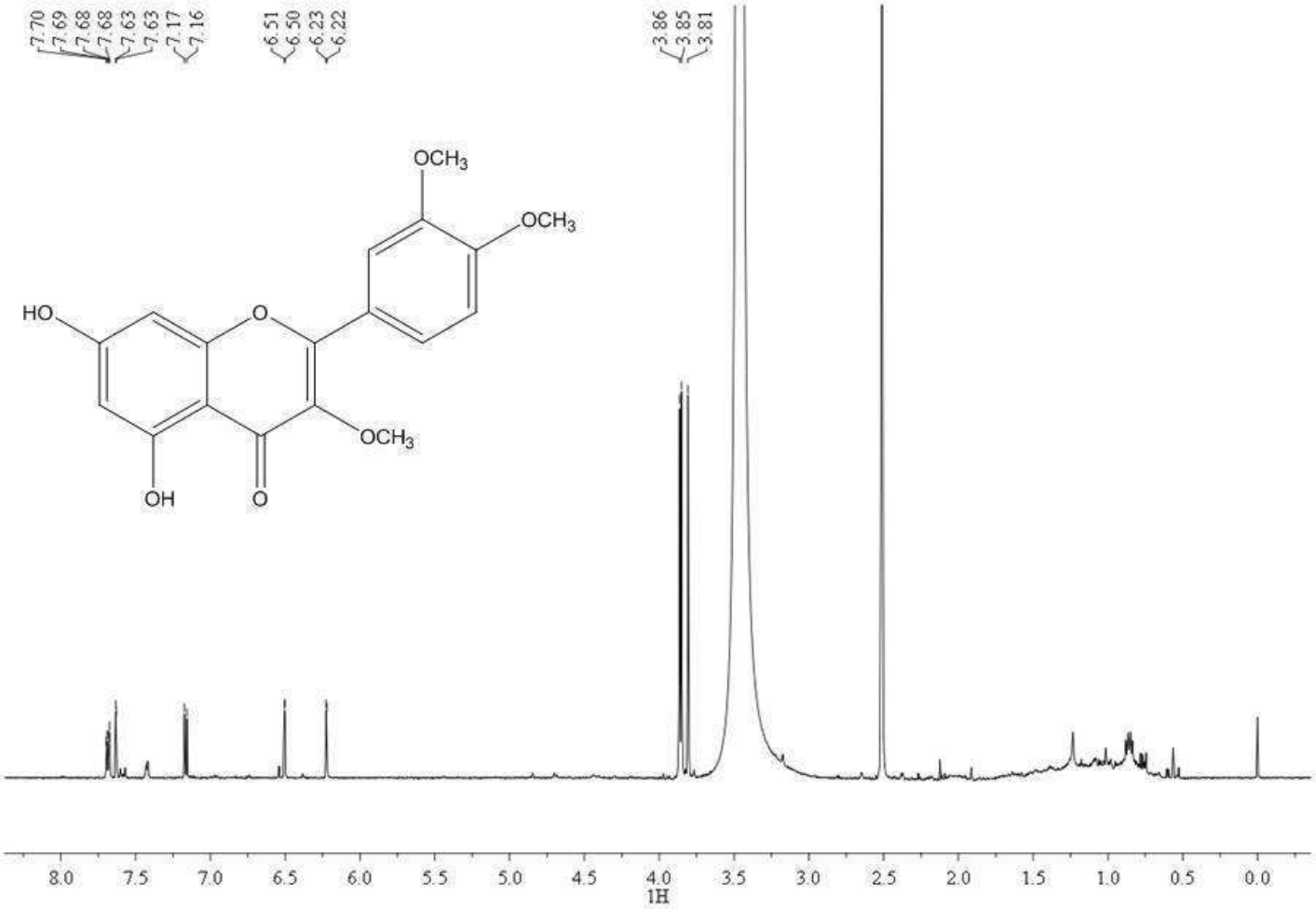

Fig. S20 ^{1}H NMR spectrum (DMSO-*d*6, 500 MHz) of 3,3',4'-tri-*O*-methyl-quercetin, **1** (**Fr-7**).

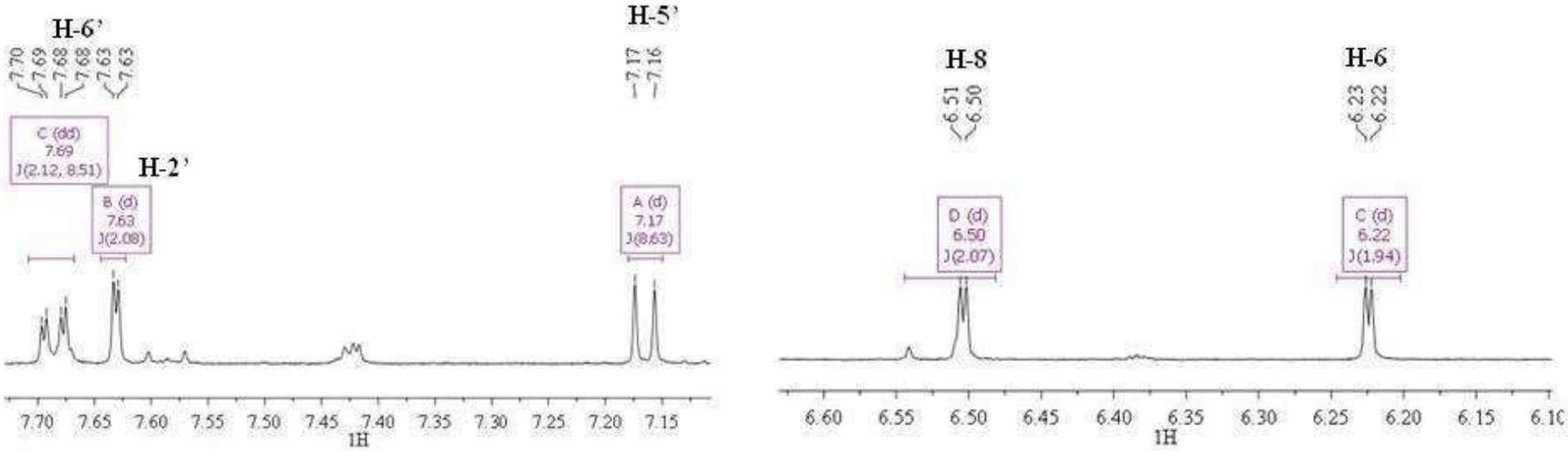

Fig. S21 ^{1}H NMR spectrum (DMSO-*d*6, 500 MHz) expanded in the aromatic protons region of 3,3',4'- tri-*O*-methyl-quercetin, **1** (**Fr-7**).

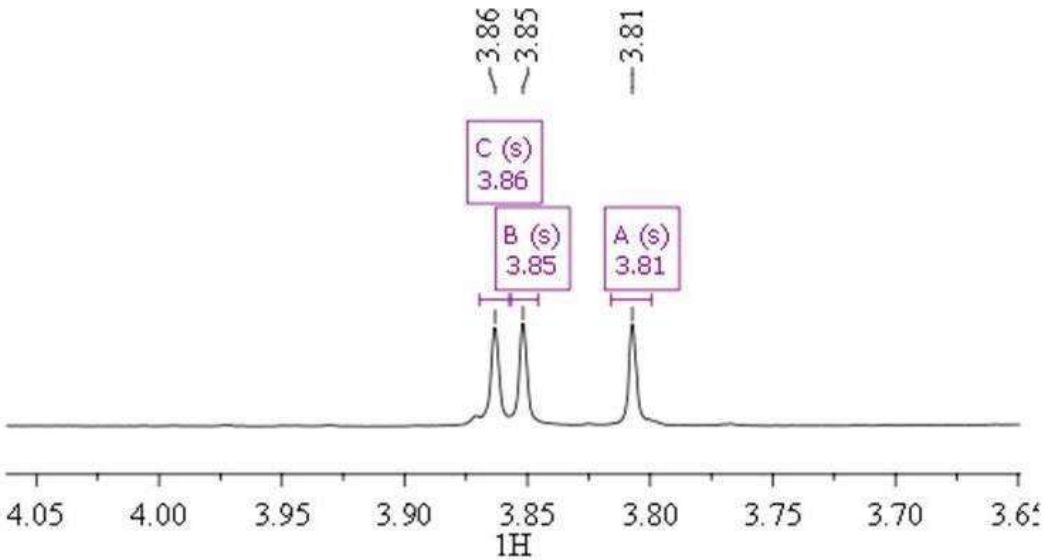

Fig. S22 ^{1}H NMR spectrum (DMSO-*d*6, 500 MHz) expanded in the region relative to methoxyl groups of 3,3',4'- tri-*O*-methyl-quercetin, **1** (**Fr-7**).

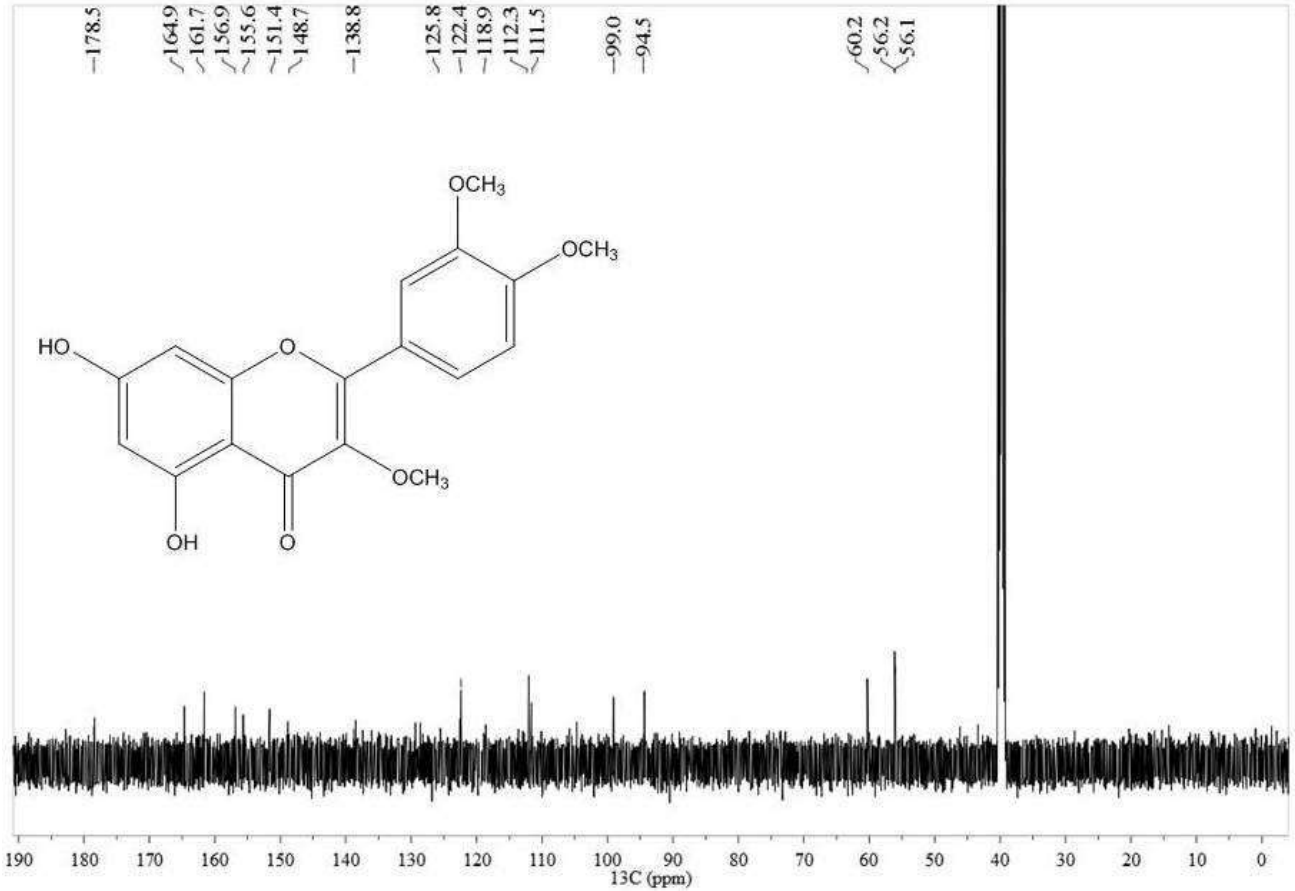

Fig. S23 ^{13}C NMR spectrum (DMSO-*d*6, 500 MHz) of 3,3',4'-tri-*O*-methyl-quercetin, **1** (**Fr-7**).

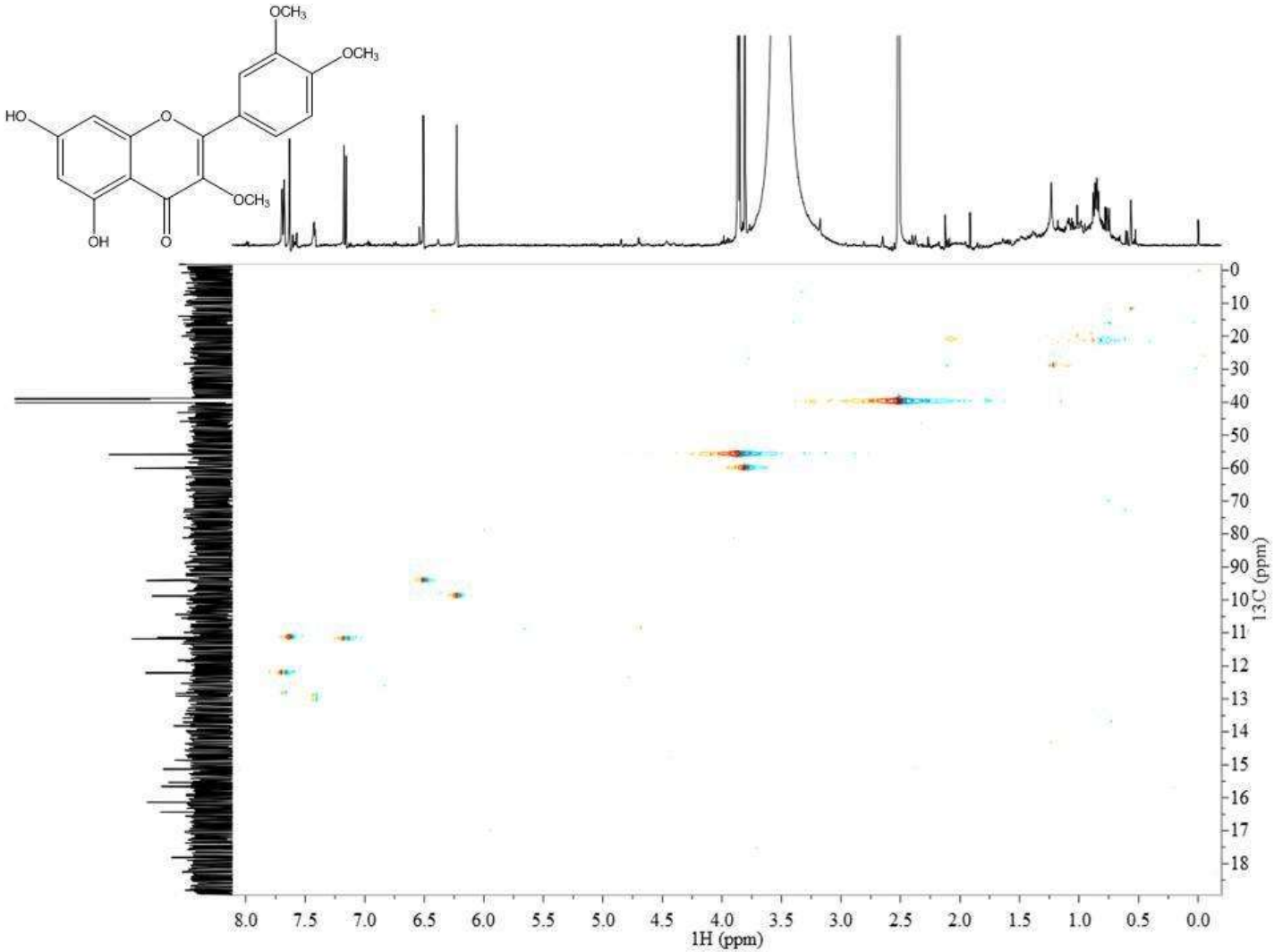

Fig. S24 HSQC ^{1}H-^{13}C NMR spectrum (DMSO-*d*6, 500 MHz) of 3,3',4'-tri-*O*-methyl-quercetin, **1** (**Fr-7**).

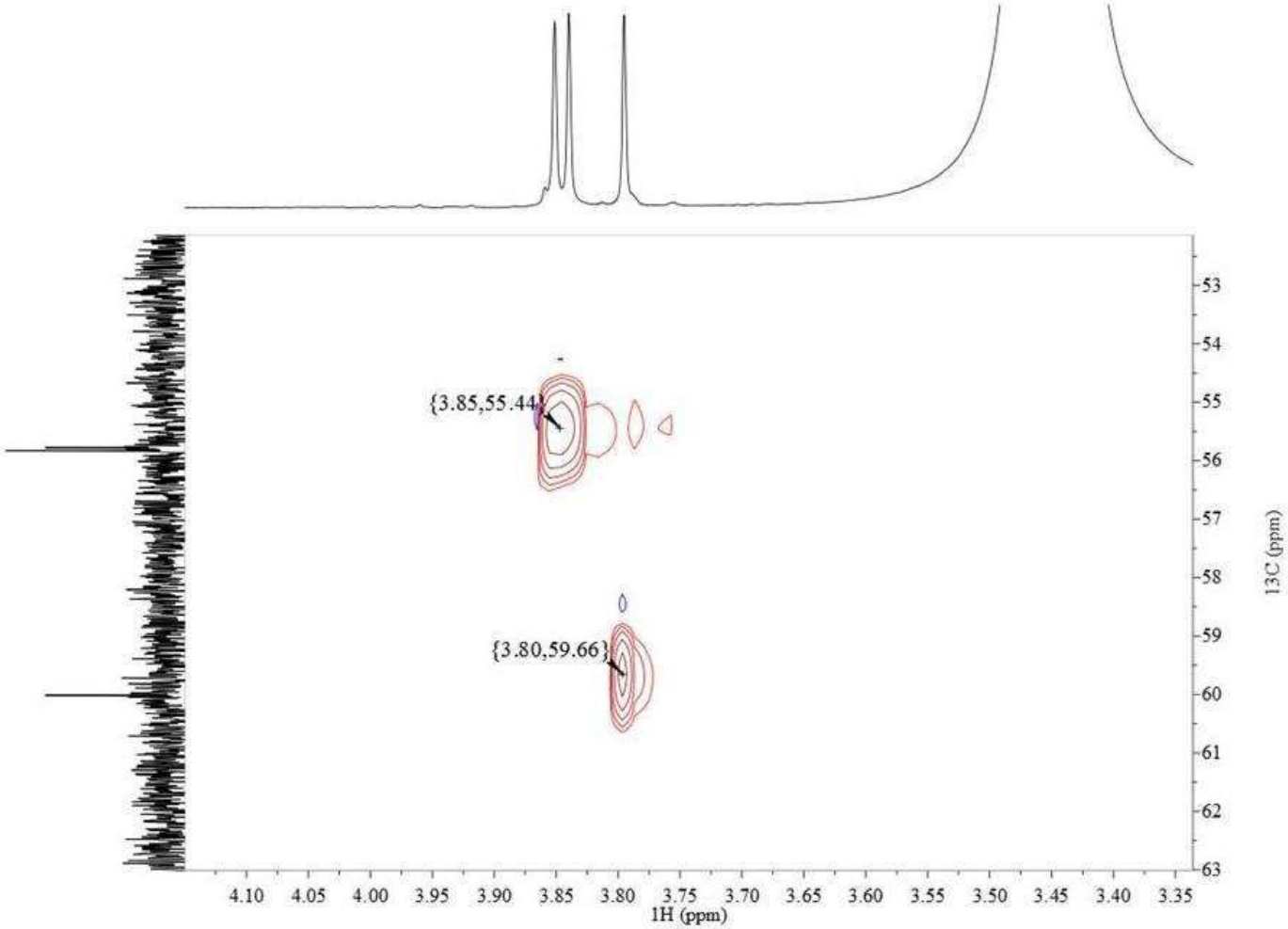

Fig. S25 HSQC ^{1}H-^{13}C NMR spectrum (DMSO-*d*6, 500 MHz) expanded in the region relative to methoxyl groups of 3,3',4'-tri-*O*-methyl-quercetin, **1** (**Fr-7**).

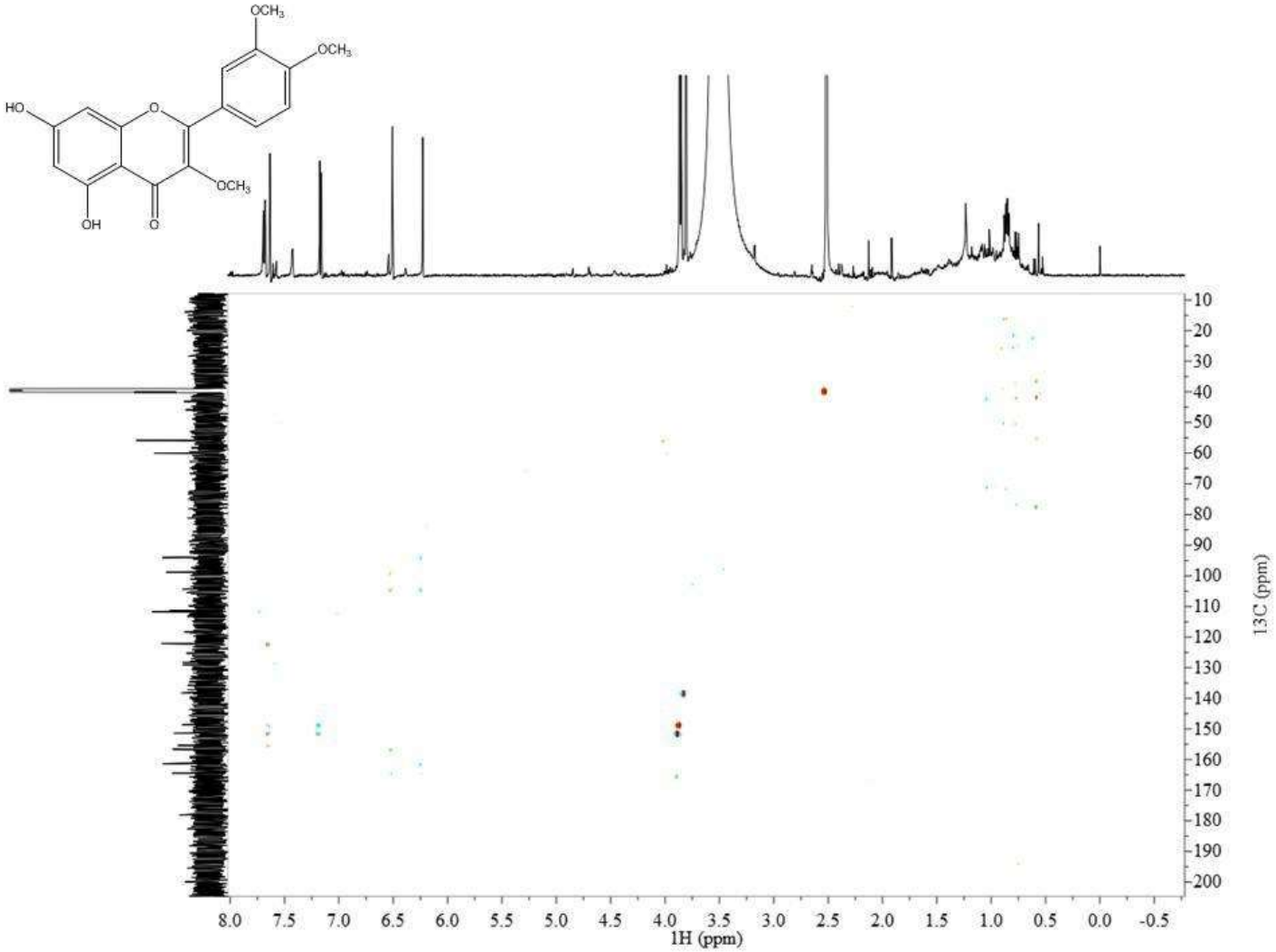

Fig. S26 HMBC ^{1}H-^{13}C NMR spectrum (DMSO-*d*6, 500 MHz) of 3,3',4'-tri-*O*-methyl-quercetin, **1** (**Fr-7**).

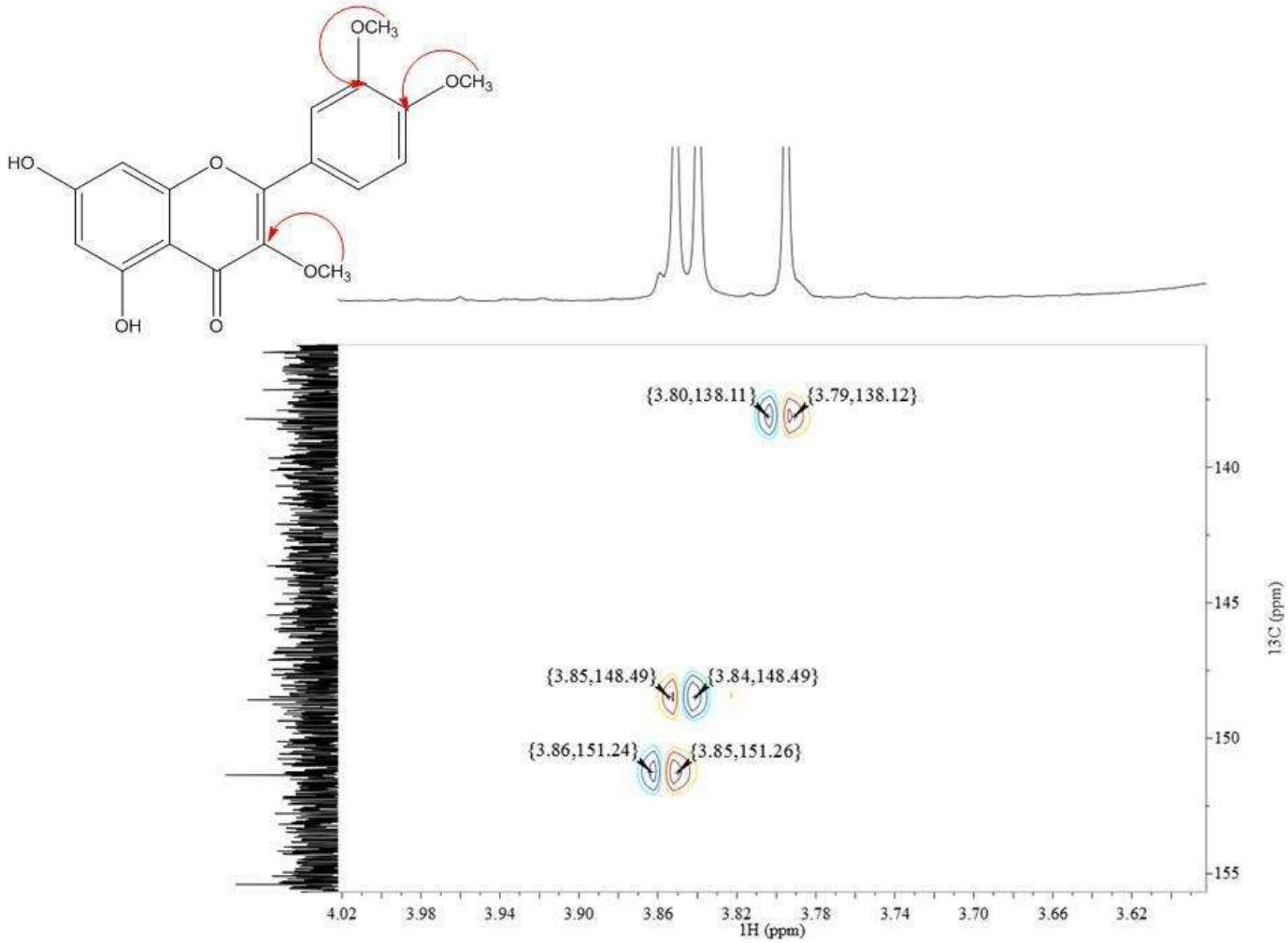

Fig. S27 HMBC ^{1}H-^{13}C NMR spectrum (DMSO-*d*6, 500 MHz) expanded in the region relative to methoxyl groups of 3,3',4'-tri-*O*-methyl-quercetin, **1** (**Fr-7**).

Table S1. ^{1}H and ^{13}C NMR spectral data for 3,3',4'-tri-*O*-methyl-quercetin, **1** (DMSO-*d*6, 500MHz) compared with the literature.

Quercetin moiety	^{1}H δ (in ppm) mult. (*J* in Hz) **Compound 1 in fraction 7**	^{1}H δ (in ppm) in $CDCl_3$ **Literature: Awad et al., 2018**	^{13}C δ (in ppm) **Compound 1 in fraction 7**
2			155.6
3			138.8
4			178.5
5			161.7
6	6.22 d (1.9)	6.40 d (2.2)	99.0
7			164.9
8	6.50 d (2.1)	6.47 d (2.2)	94.5
9			156.9
10			111.5
1'			122.4
2'	7.63 d (2.1)	7.78 d (2.0)	112.3
3'			148.7
4'			151.4
5'	7.17 d (8.6)	7.12 d (8.4)	118.9
6'	7.69 dd (8.5, 2.1)	7.66 dd (8.4, 2.2)	125.8

3-OCH_3	3.81 s	3.84 s	60.2
3’-OCH_3	3.85 s	3.86 s	56.1
4’-OCH_3	3.86 s	3.96 s	56.2

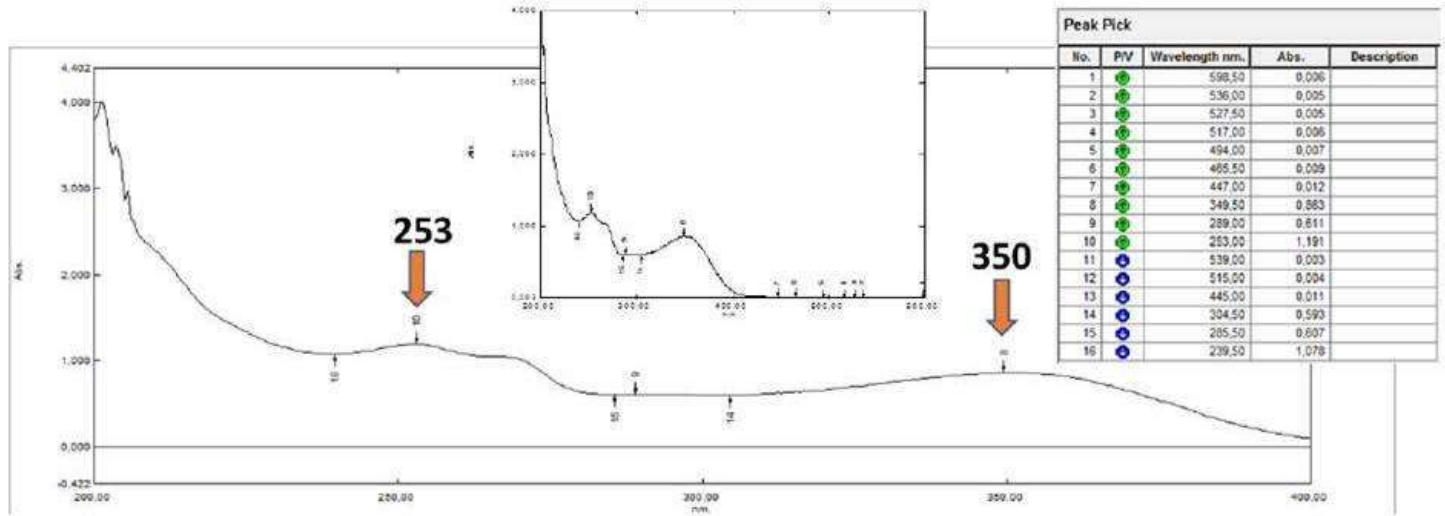

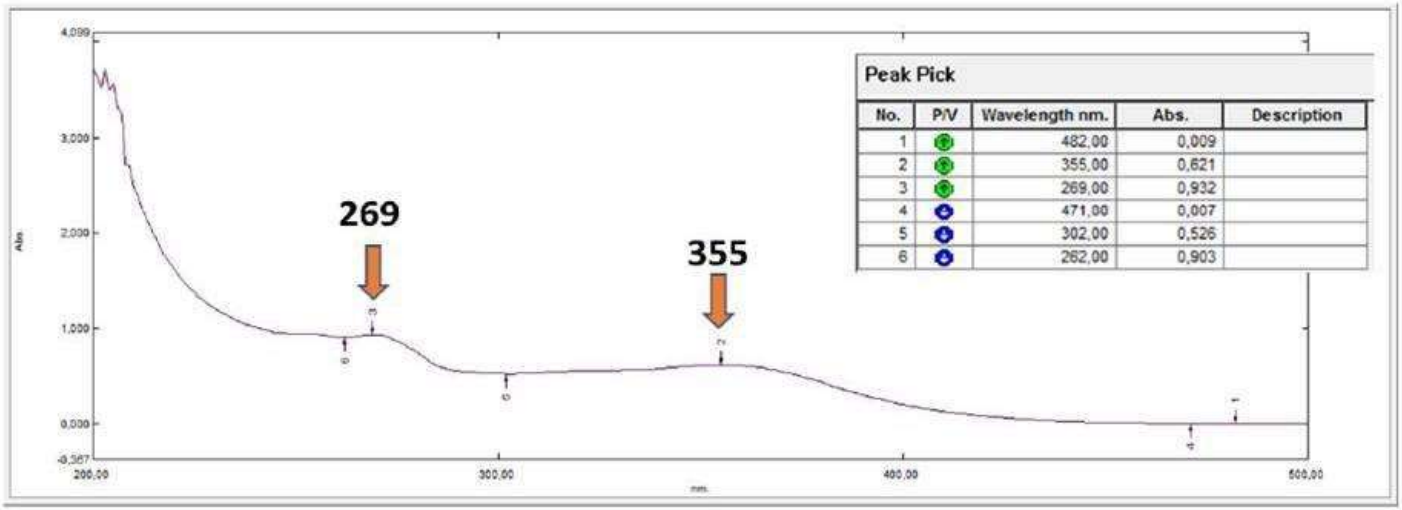

Fig. S28 Ultraviolet spectrum of 3,3’,4’-tri-*O*-methyl-quercetin, **1** (**Fr-7**).

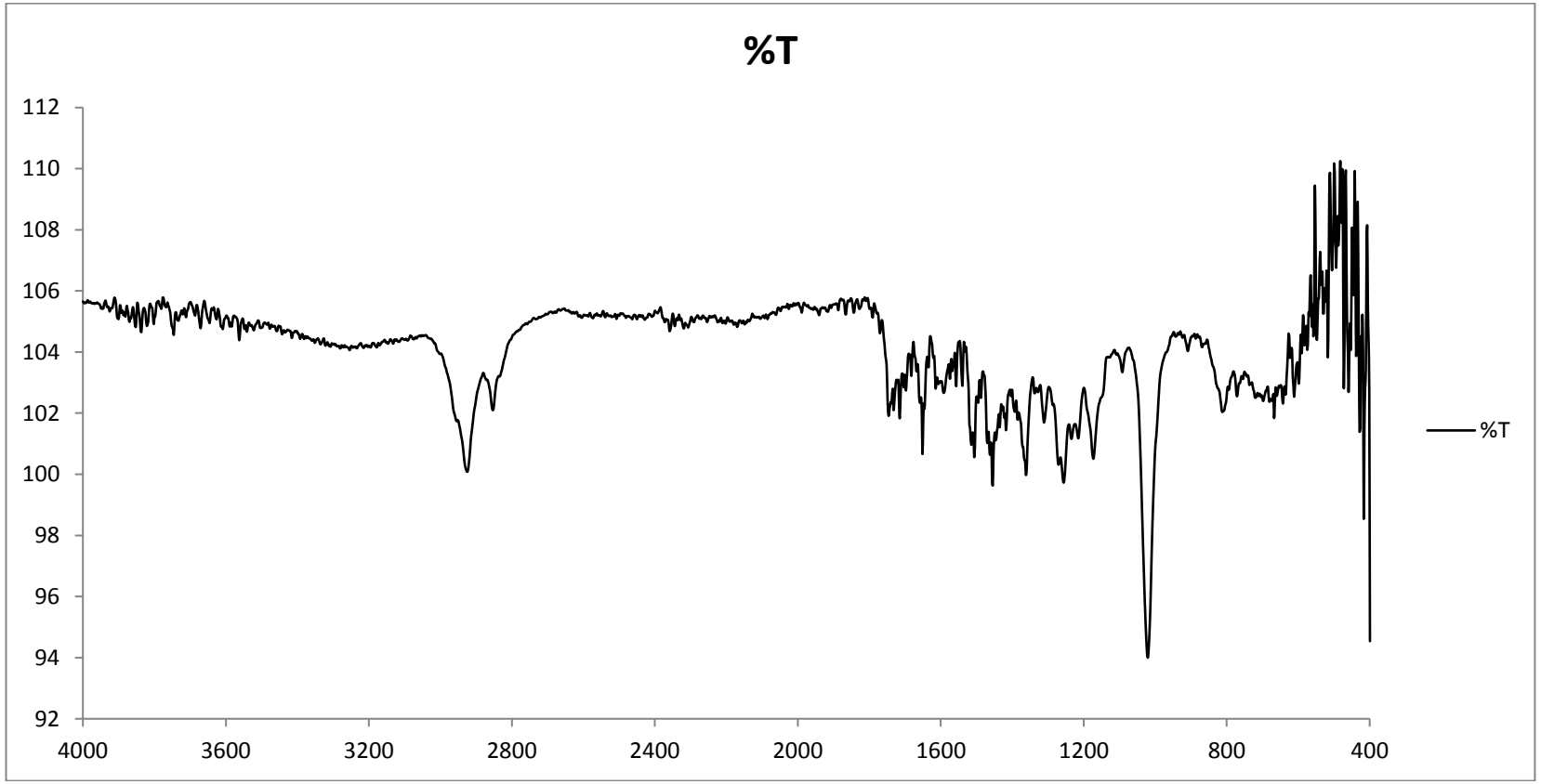

Fig. S29 Infrared spectrum (KBr) of 3,3',4'-tri-*O*-methyl-quercetin, **1** (**Fr-7**).

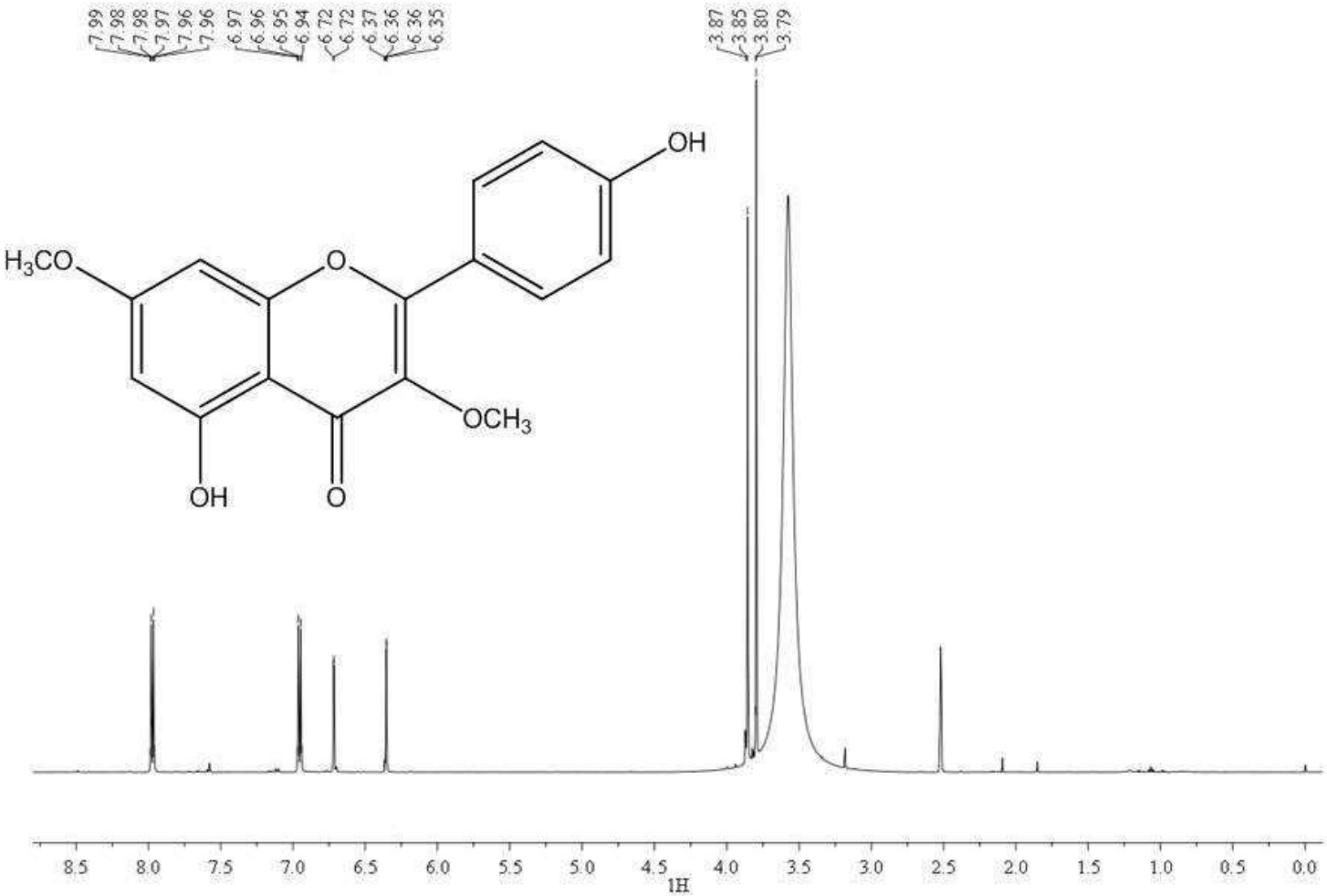

Fig. S30 ^{1}H NMR spectrum (DMSO-*d*6, 500 MHz) of 3,7-di-*O*-methyl-kaempferol (kumatakenin), **3** (**Fr-10**).

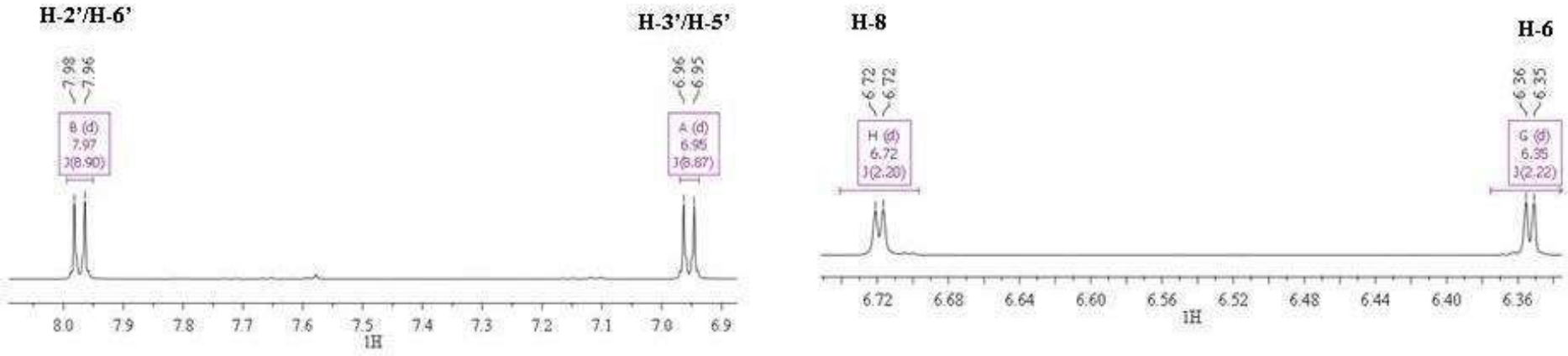

Fig. S31 ^{1}H NMR spectrum (DMSO-*d*6, 500 MHz) expanded in the aromatic protons region of 3,7-di-*O*-methyl-kaempferol (kumatakenin), **3** (**Fr-10**).

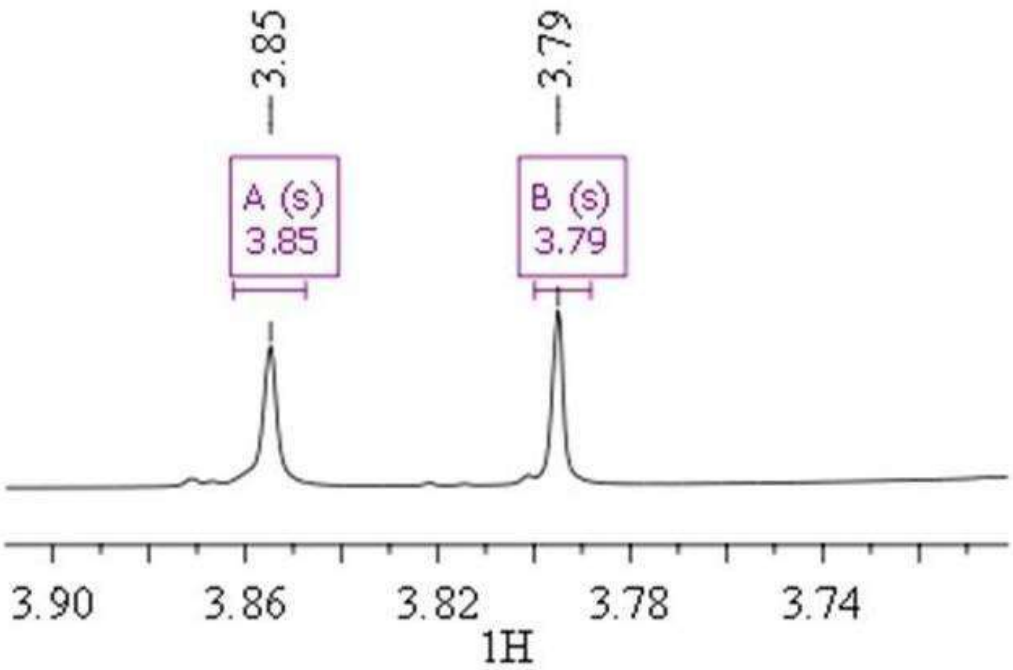

Fig. S32 ^{1}H NMR spectrum (DMSO-*d*6, 500 MHz) expanded in the region relative to methoxyl groups of 3,7-di-*O*-methyl-kaempferol (kumatakenin), **3** (**Fr-10**).

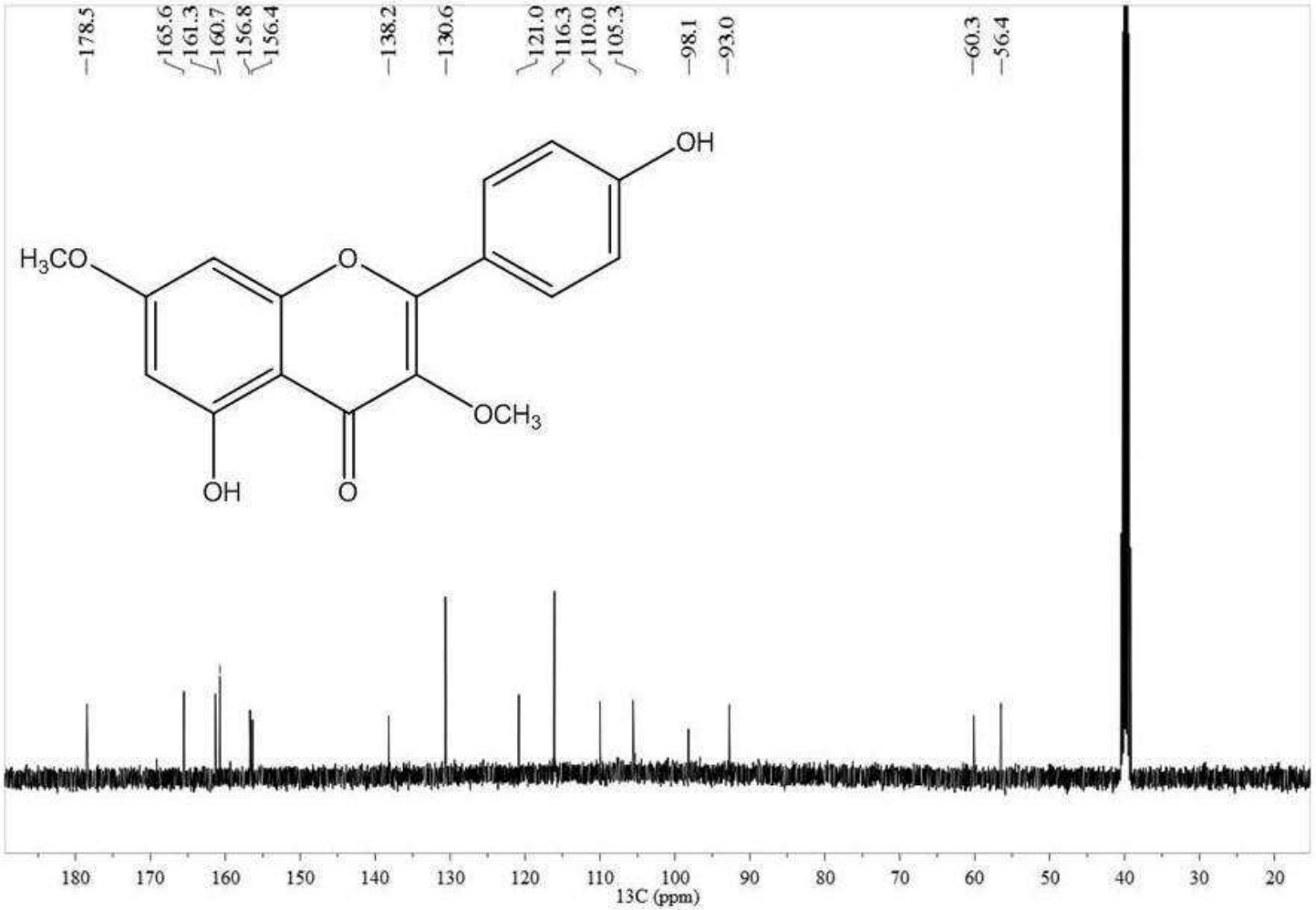

Fig. S33 ^{13}C NMR spectrum (DMSO-*d*6, 500 MHz) of 3,7-di-*O*-methyl-kaempferol (kumatakenin), **3** (**Fr-10**).

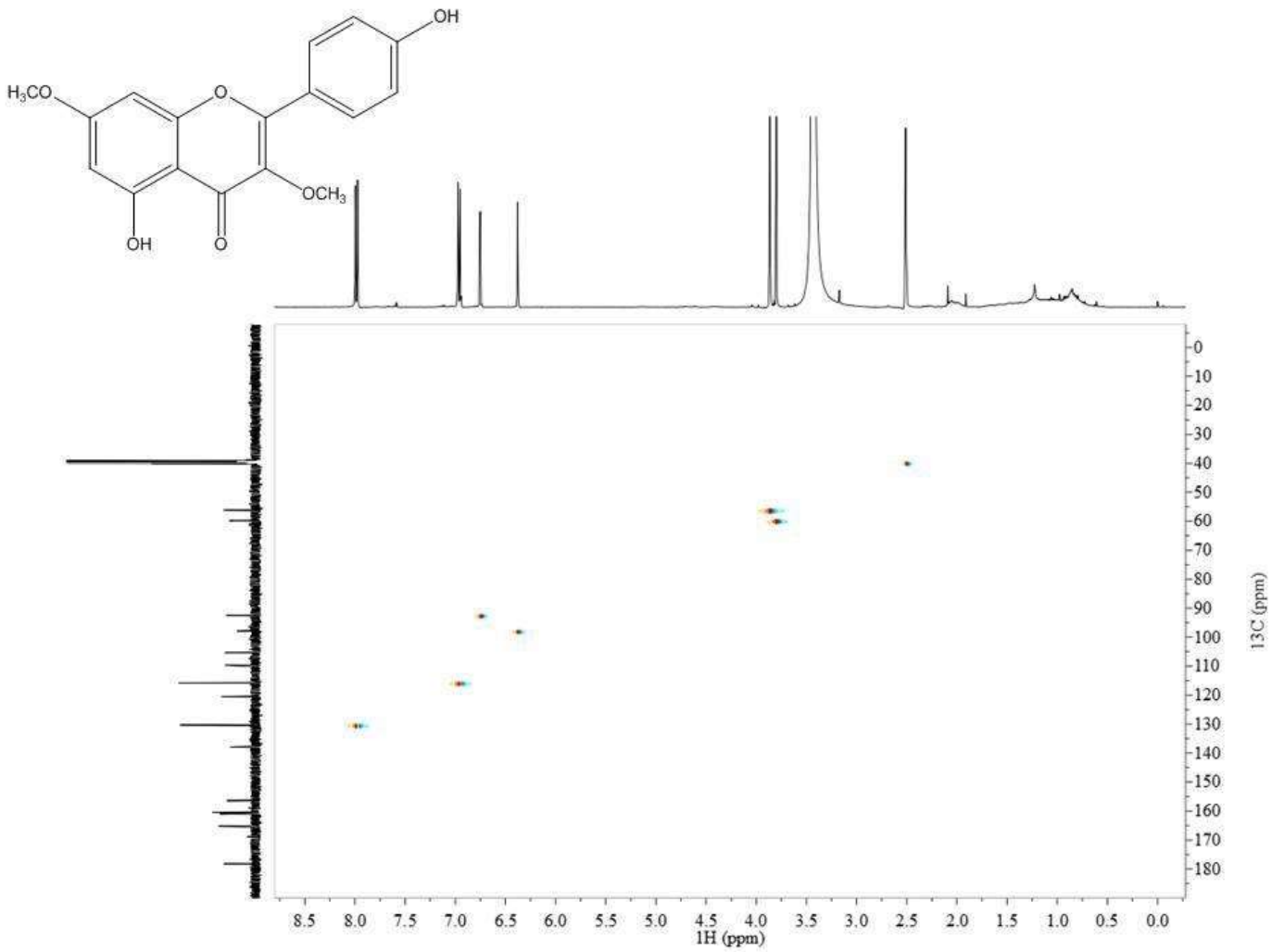

Fig. S34 HSQC ^{1}H-^{13}C NMR spectrum (DMSO-*d*6, 500 MHz) of 3,7-di-*O*-methyl-kaempferol (kumatakenin), **3** (**Fr-10**).

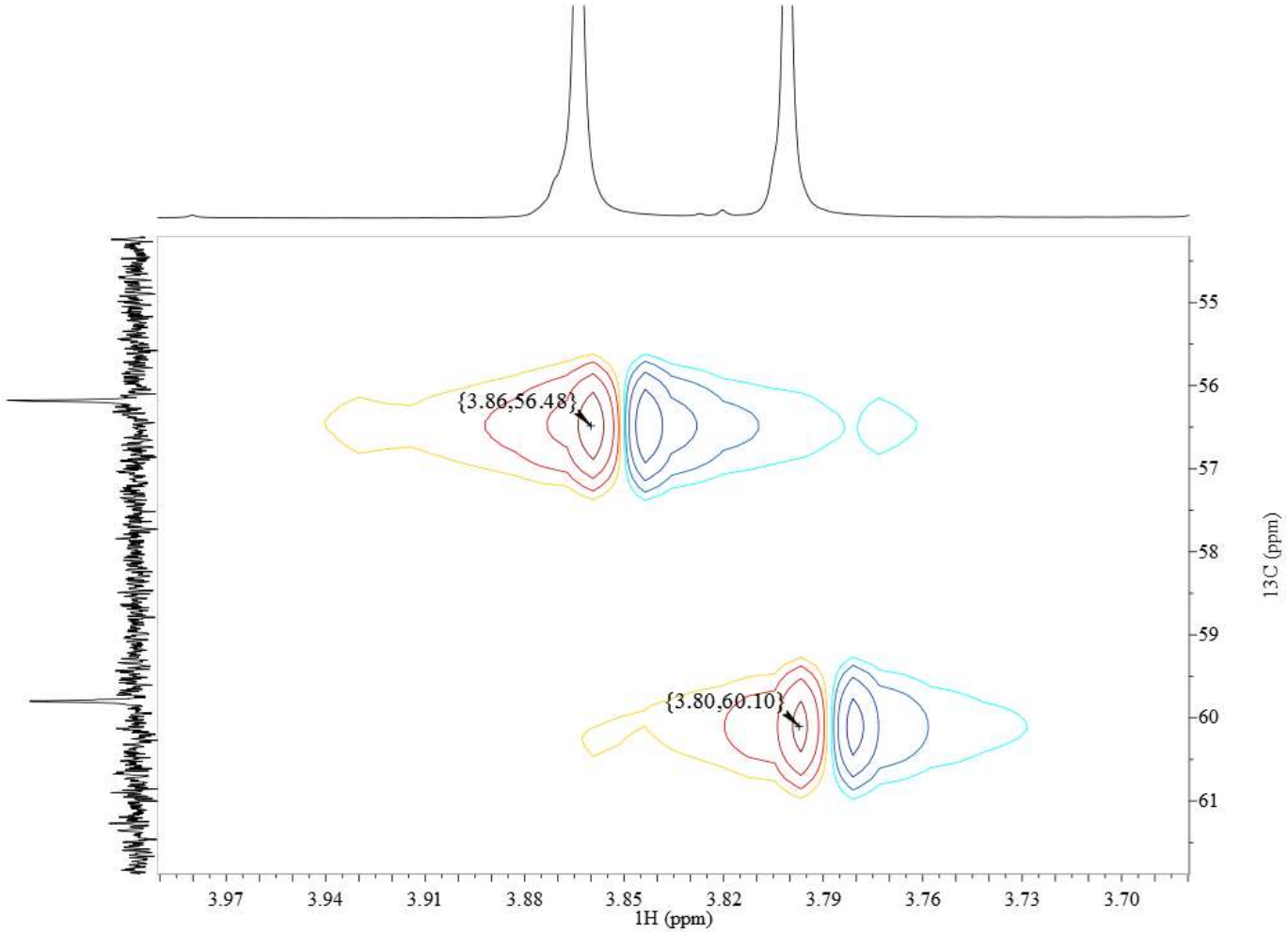

Fig. S35 HSQC ^{1}H-^{13}C NMR spectrum (DMSO-*d*6, 500 MHz) expanded in the region relative to methoxyl groups of 3,7-di-*O*-methyl-kaempferol (kumatakenin), **3** (**Fr-10**).

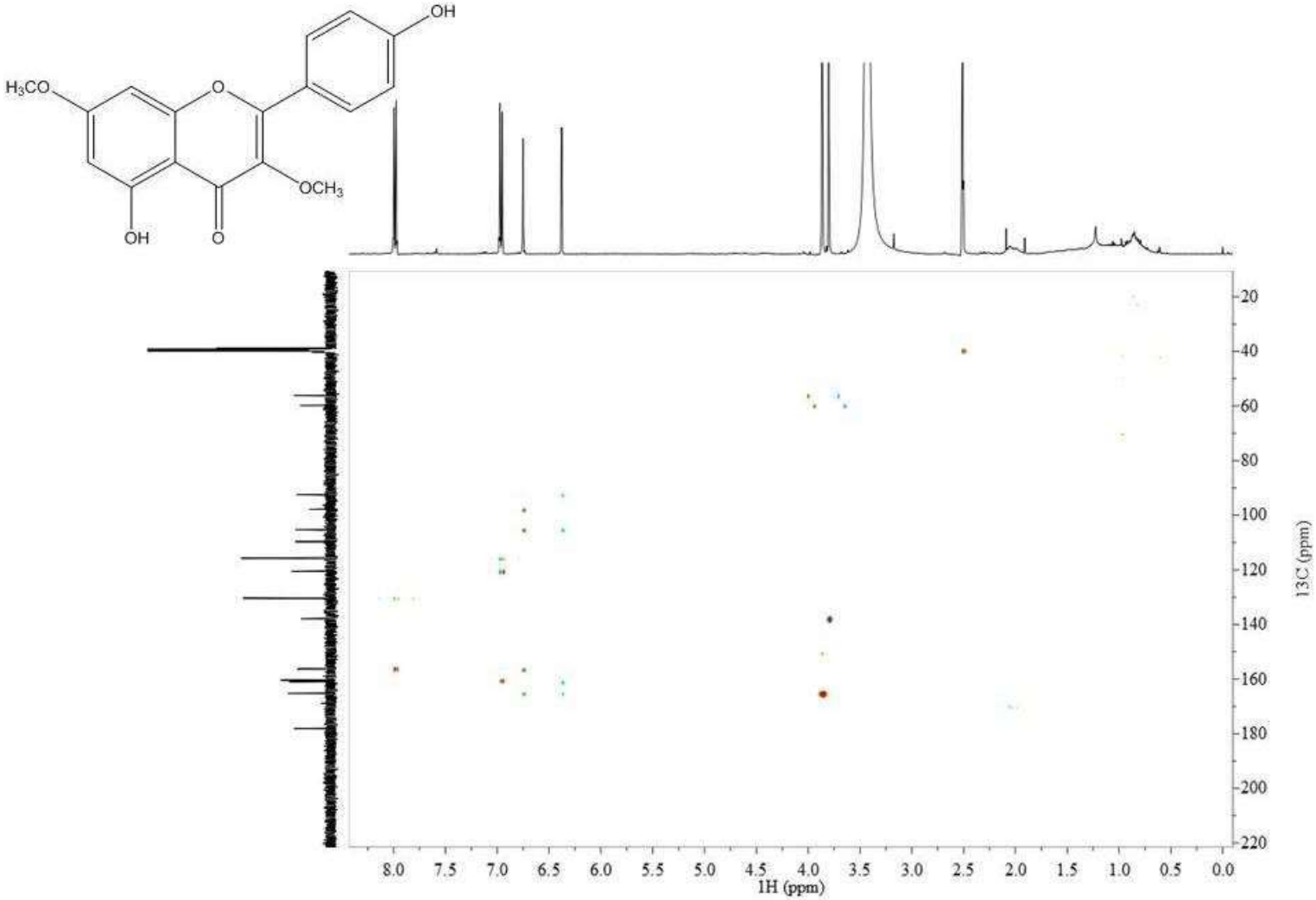

Fig. S36 HMBC ^{1}H-^{13}C NMR spectrum (DMSO-*d*6, 500 MHz) of 3,7-di-*O*-methyl-kaempferol (kumatakenin), **3** (**Fr-10**).

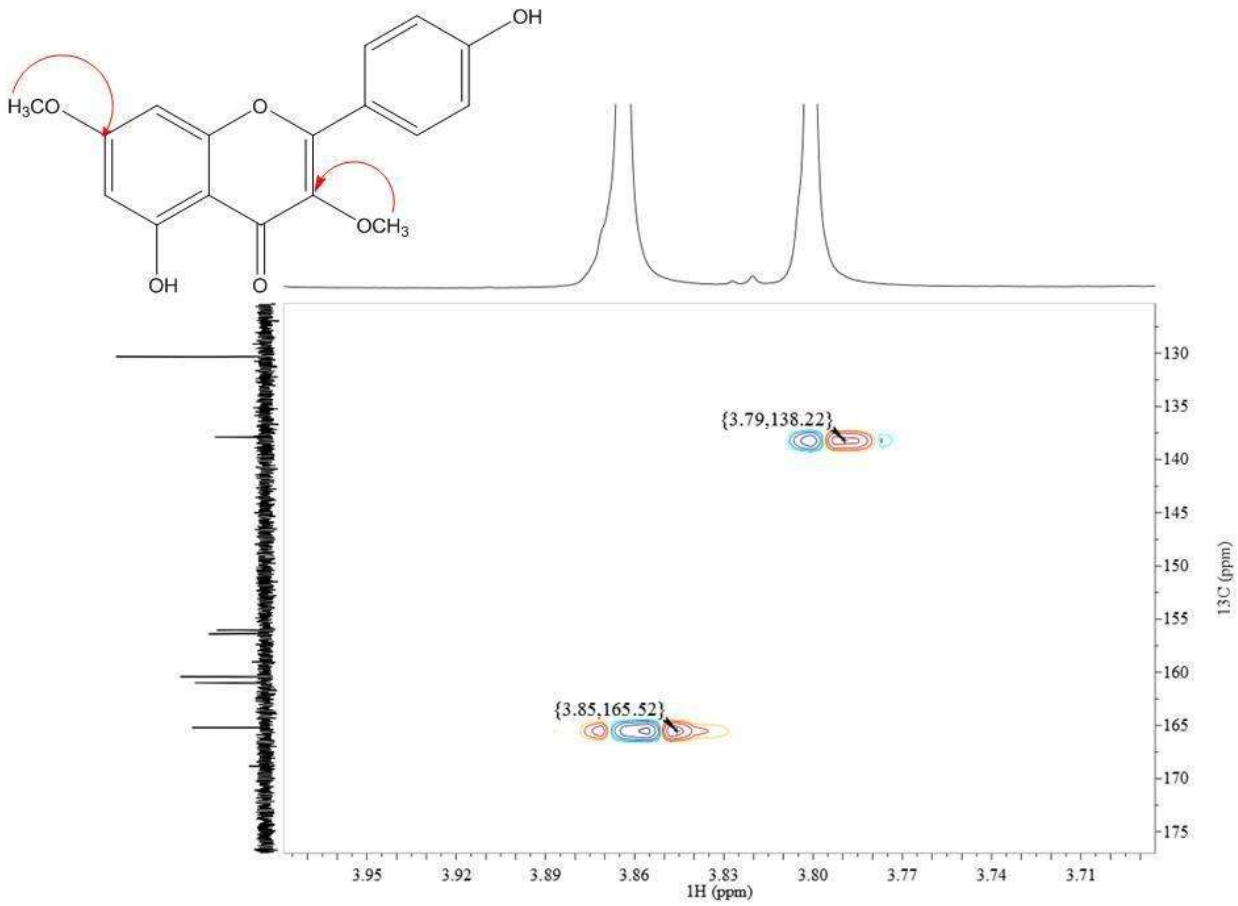

Fig. S37 HMBC ^{1}H-^{13}C NMR spectrum (DMSO-*d*6, 500 MHz) expanded in the region relative to methoxyl groups of 3,7-di-*O*-methyl-kaempferol (kumatakenin), **3** (**Fr-10**).

Table S2. ^{1}H and ^{13}C NMR spectral data for 3,7-di-*O*-methyl-kaempferol (kumatakenin), **3** (DMSO-*d*6, 500MHz) compared with the literature.

	^{1}H δ (in ppm) mult. (*J* in Hz) **Compound 3 in fraction 10**	^{1}H δ (in ppm) in DMSO-*d*6 **Literature: Silva et al., 2009**	^{13}C δ (in ppm) **Compound 3 in fraction 10**	^{13}C δ (in ppm) in DMSO-*d*6 **Literature: Silva et al., 2009**
kaempferol moiety				
2			161.3	155.95
3			138.2	137.86
4			178.5	178.09
5			160.7	160.96
6	6.35 d (2.2)	6.35 sl	98.1	97.77
7			165.6	165.13
8	6.72 d (2.2)	6.74 sl	93.0	92.37
9			156.4	156.33
10			105.3	105.21
1’			121.0	120.52
2’,6’	7.98 d (8.9)	7.96 d	130.6	130.24
3’,5’	6.96 d (8.8)	8.67 d	116.3	115.68
4’			156.8	160.29
3-OCH_3	3.79 s	3.78 s	60.3	59.72
7-OCH_3	3.85 s	3.84 s	56.4	56.10

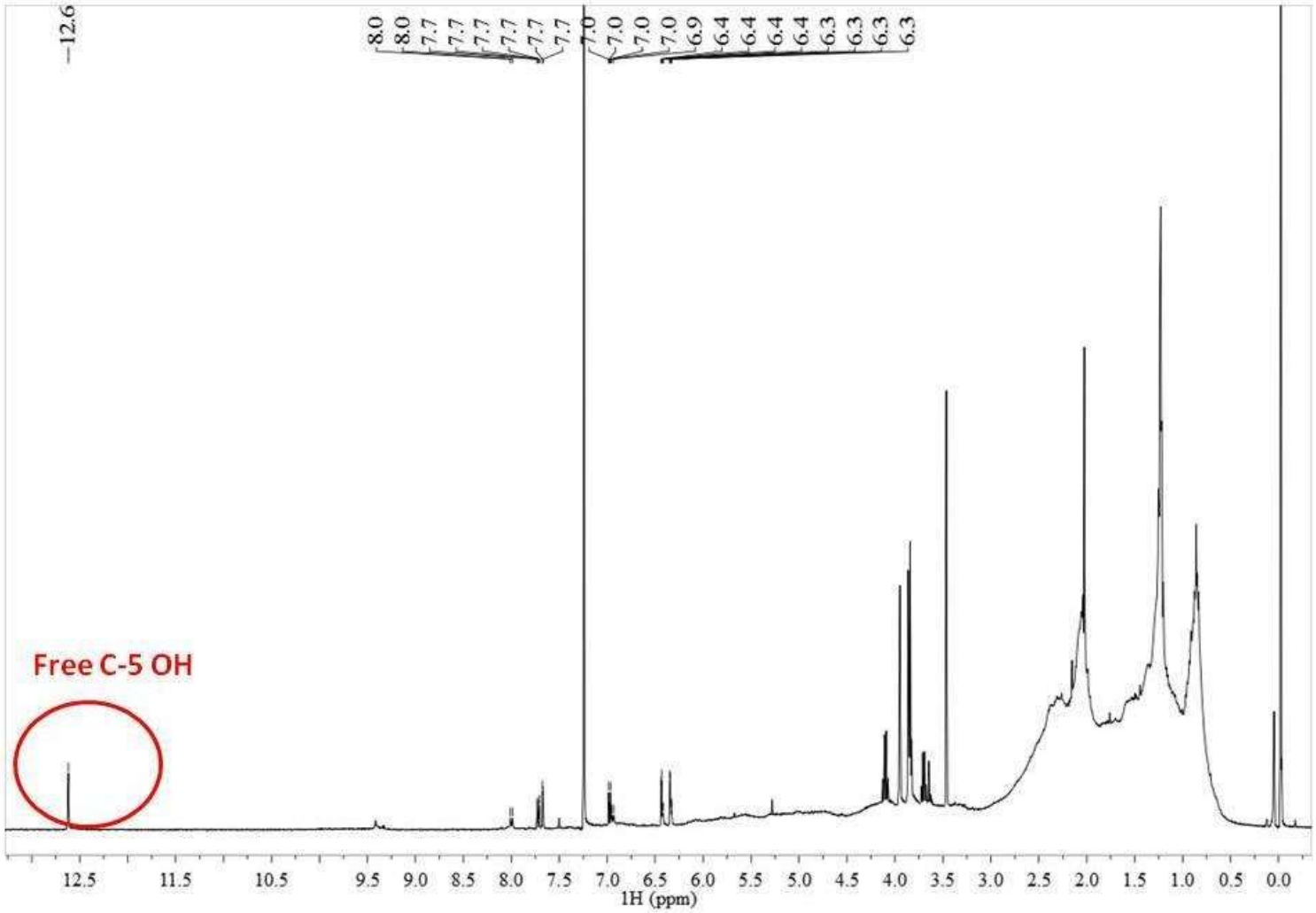

Fig. S38 ^{1}H NMR spectrum ($CdCl_3$, 500 MHz) of mixture of 3,7-di-*O*-methyl-kaempferol (kumatakenin), (**3**) and tetra-*O*-methyl-quercetin (retusin) (**2**) (**Fr-11**).

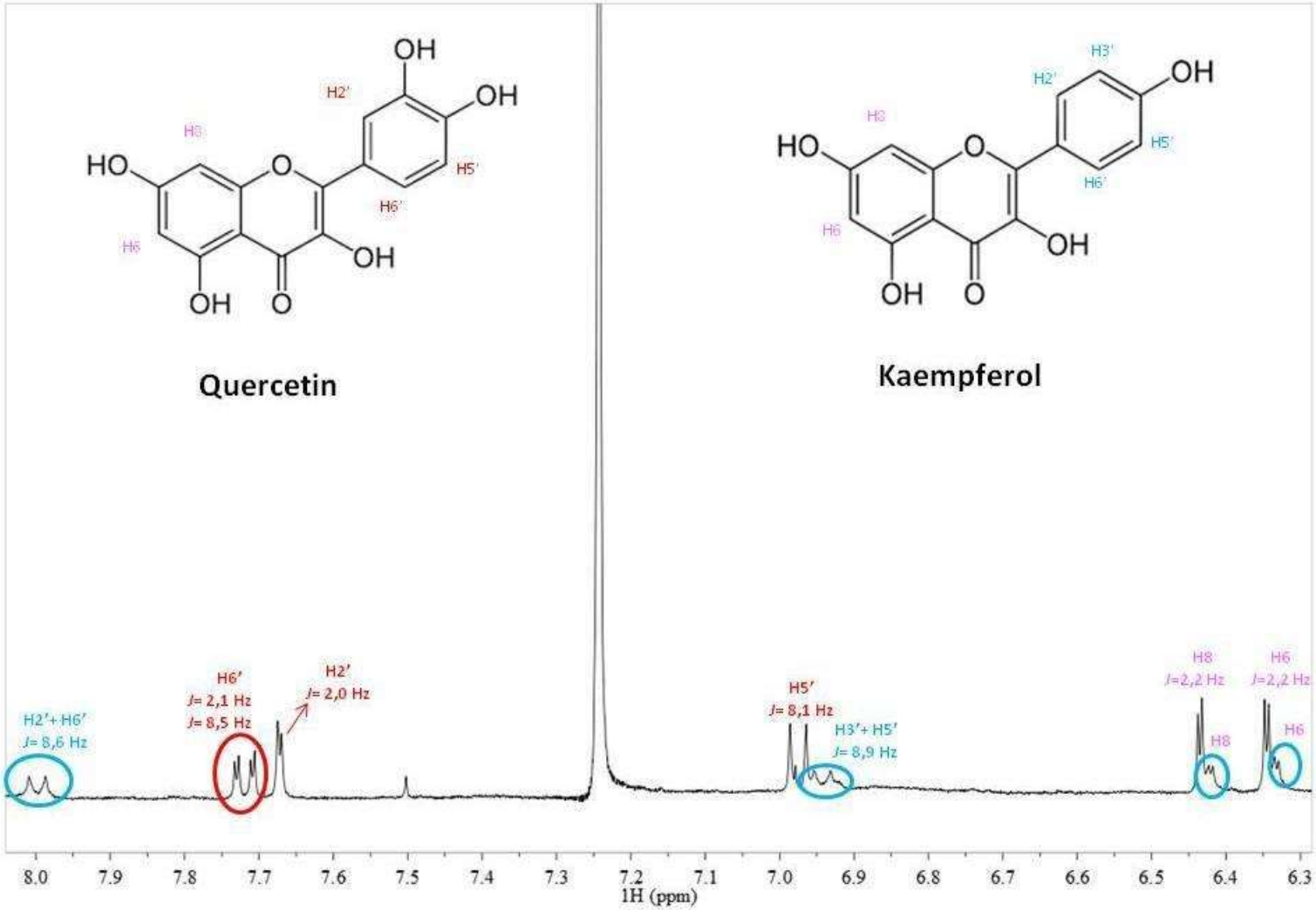

Fig. S39 ^{1}H NMR spectrum ($CdCl_3$, 500 MHz) expanded in the region relative to the aromatic protons (**Fr-11**).

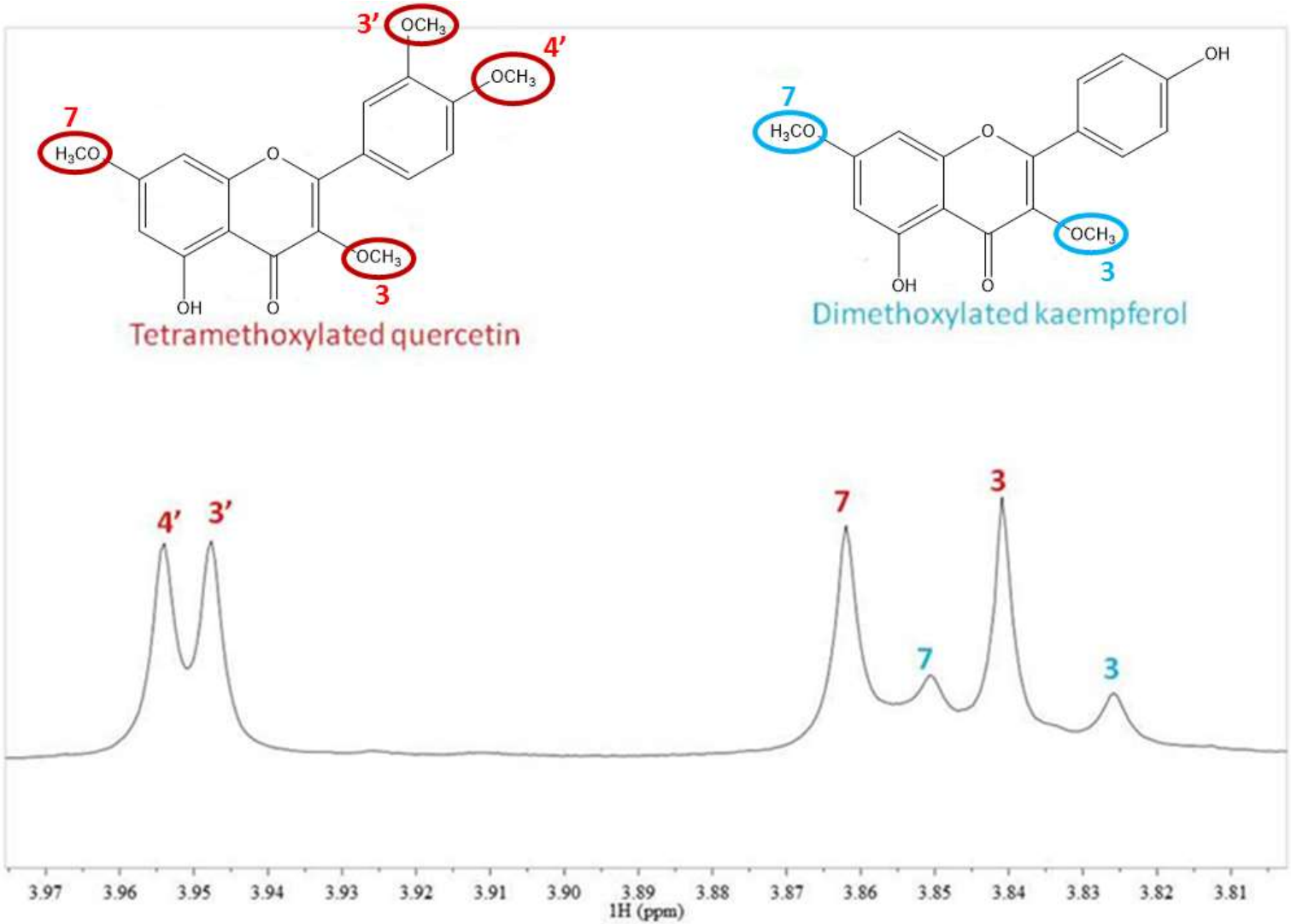

Fig. S40 ^{1}H NMR spectrum ($CdCl_3$, 500 MHz) expanded in the region relative to methoxyl groups (**Fr-11**).

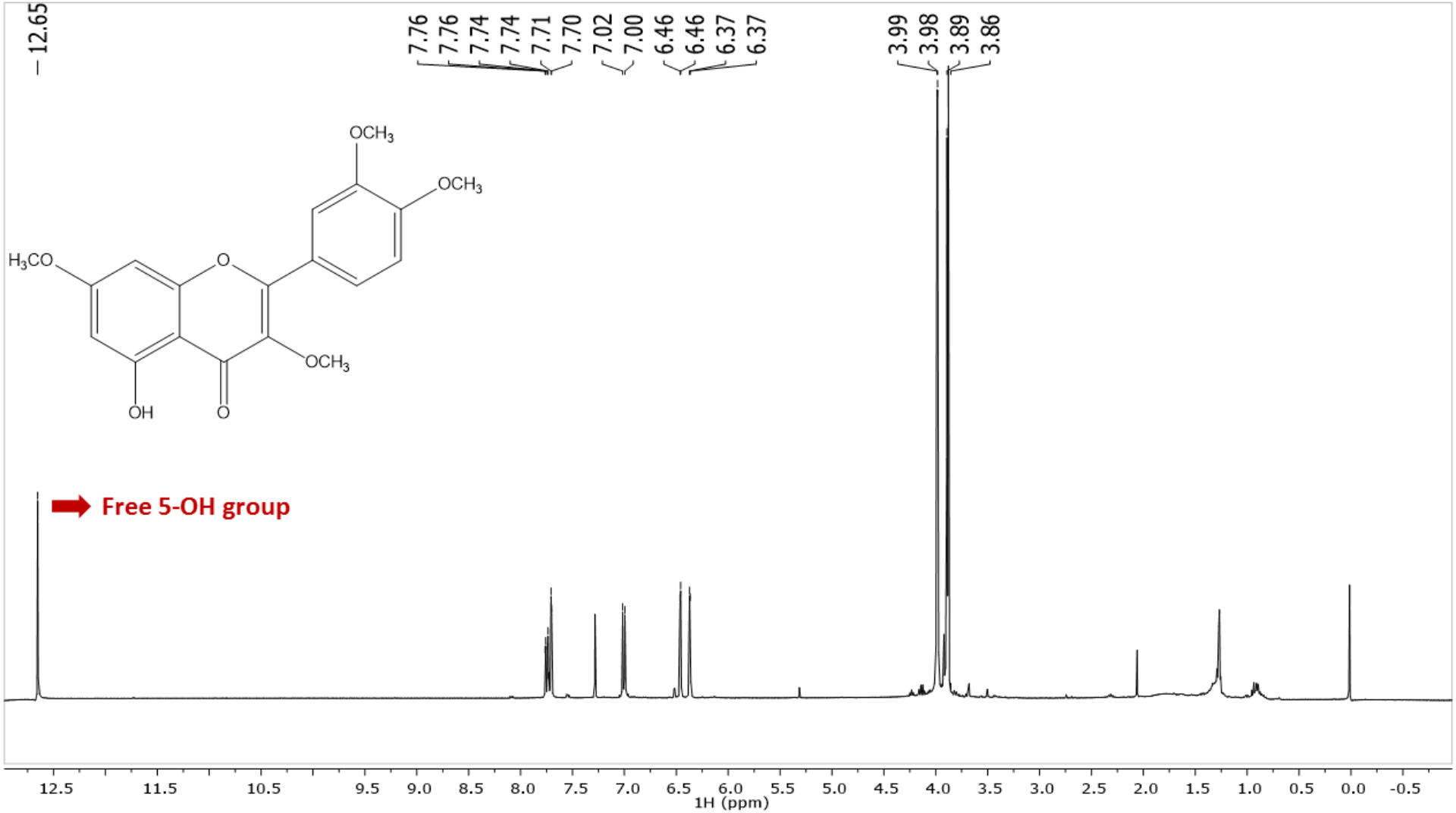

Fig. S41 ^{1}H NMR spectrum ($CdCl_3$, 500 MHz) of tetra-*O*-methyl-quercetin (retusin), (**2**) (**Fr-11A**).

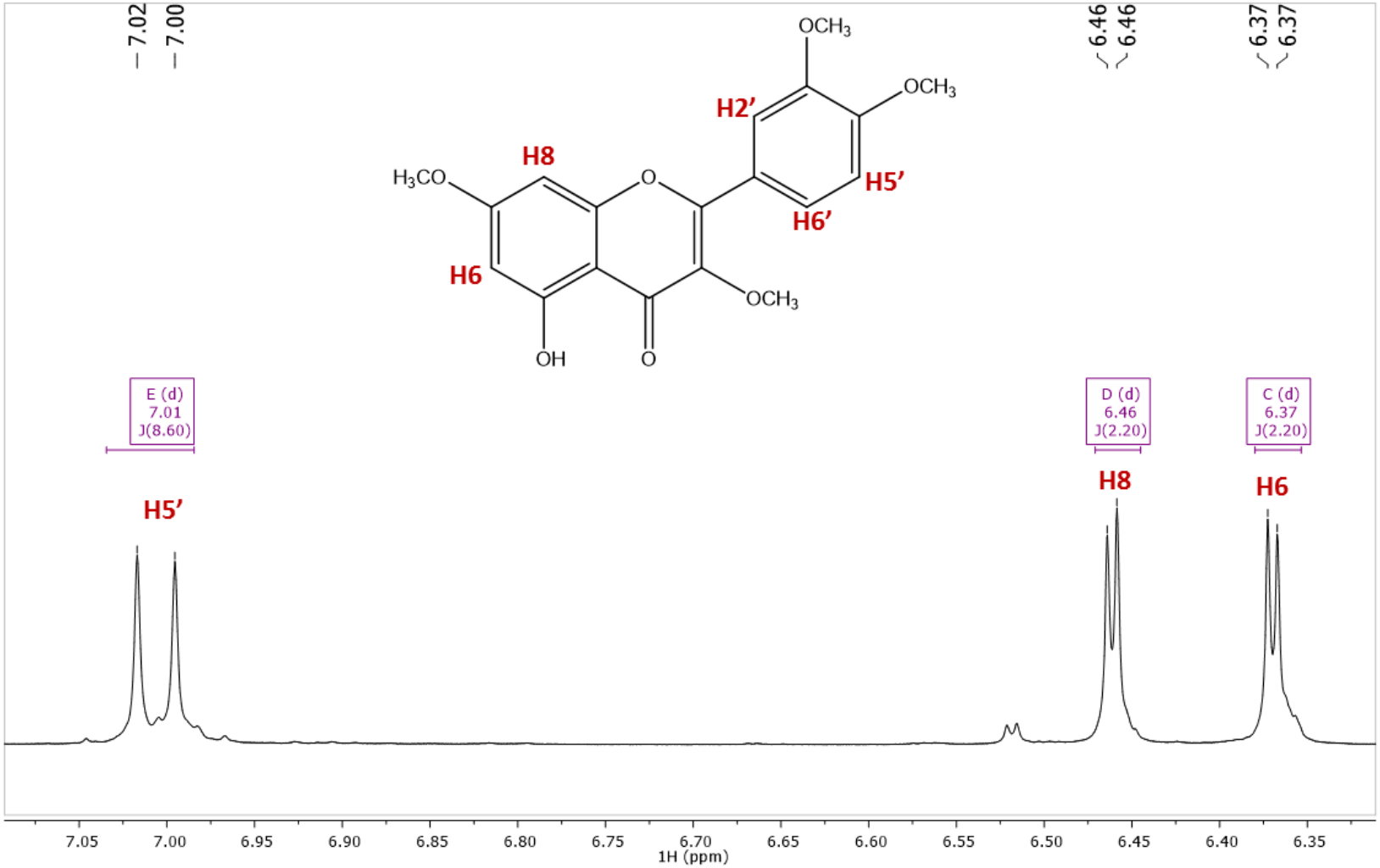

Fig. S42 ^{1}H NMR spectrum ($CdCl_3$, 500 MHz) expanded in the aromatic protons region of tetra-*O*-methyl-quercetin (retusin), (**2**) (**Fr-11A**).

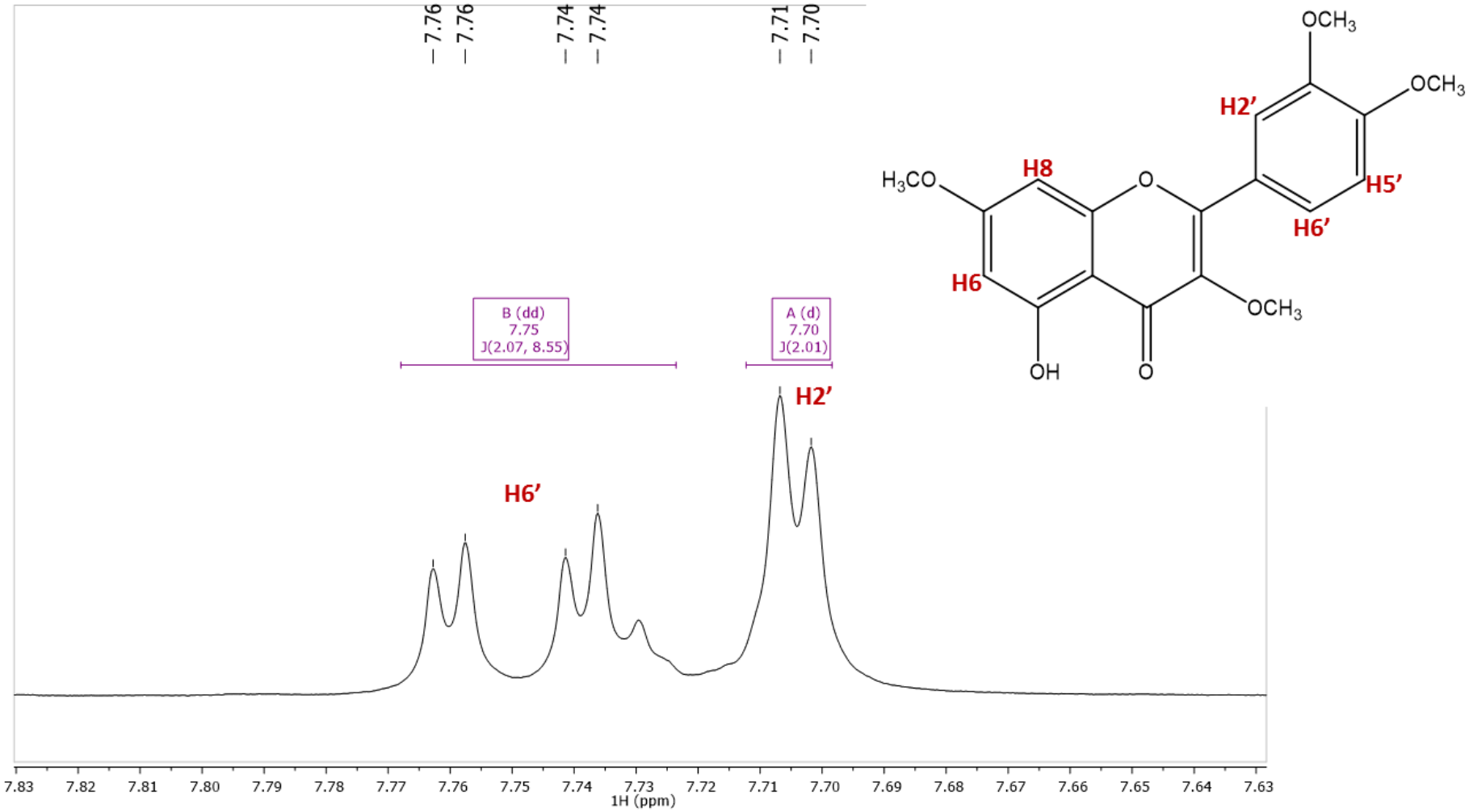

Fig. S43 ^{1}H NMR spectrum ($CdCl_3$, 500 MHz) expanded in the aromatic protons region of tetra-*O*-methyl-quercetin (retusin), (**2**) (**Fr-11A**).

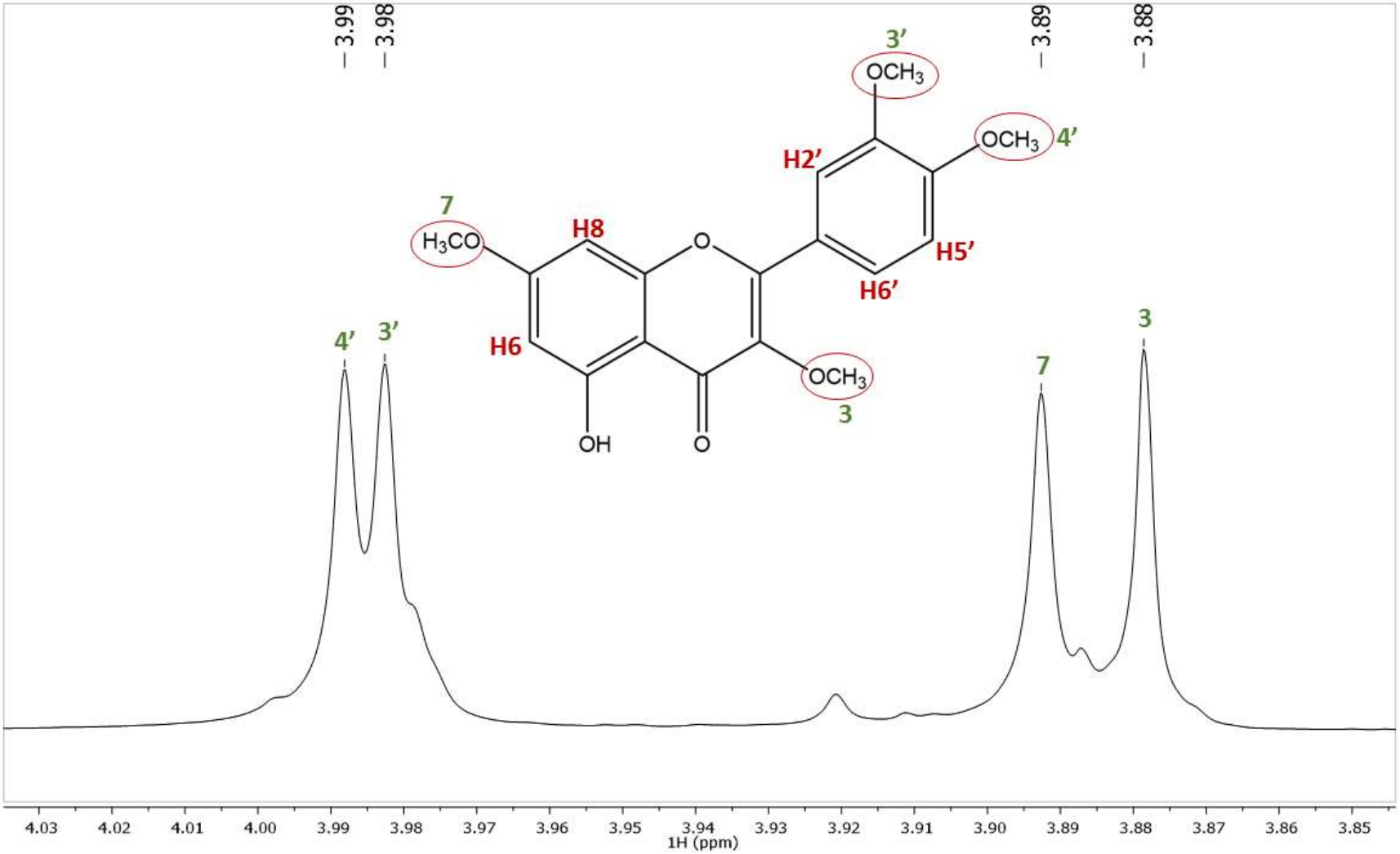

Fig. S44 ^{1}H NMR spectrum ($CdCl_3$, 500 MHz) expanded in the region relative to methoxyl groups of tetra-*O*-methyl-quercetin (retusin), (**2**) (**Fr-11A**).

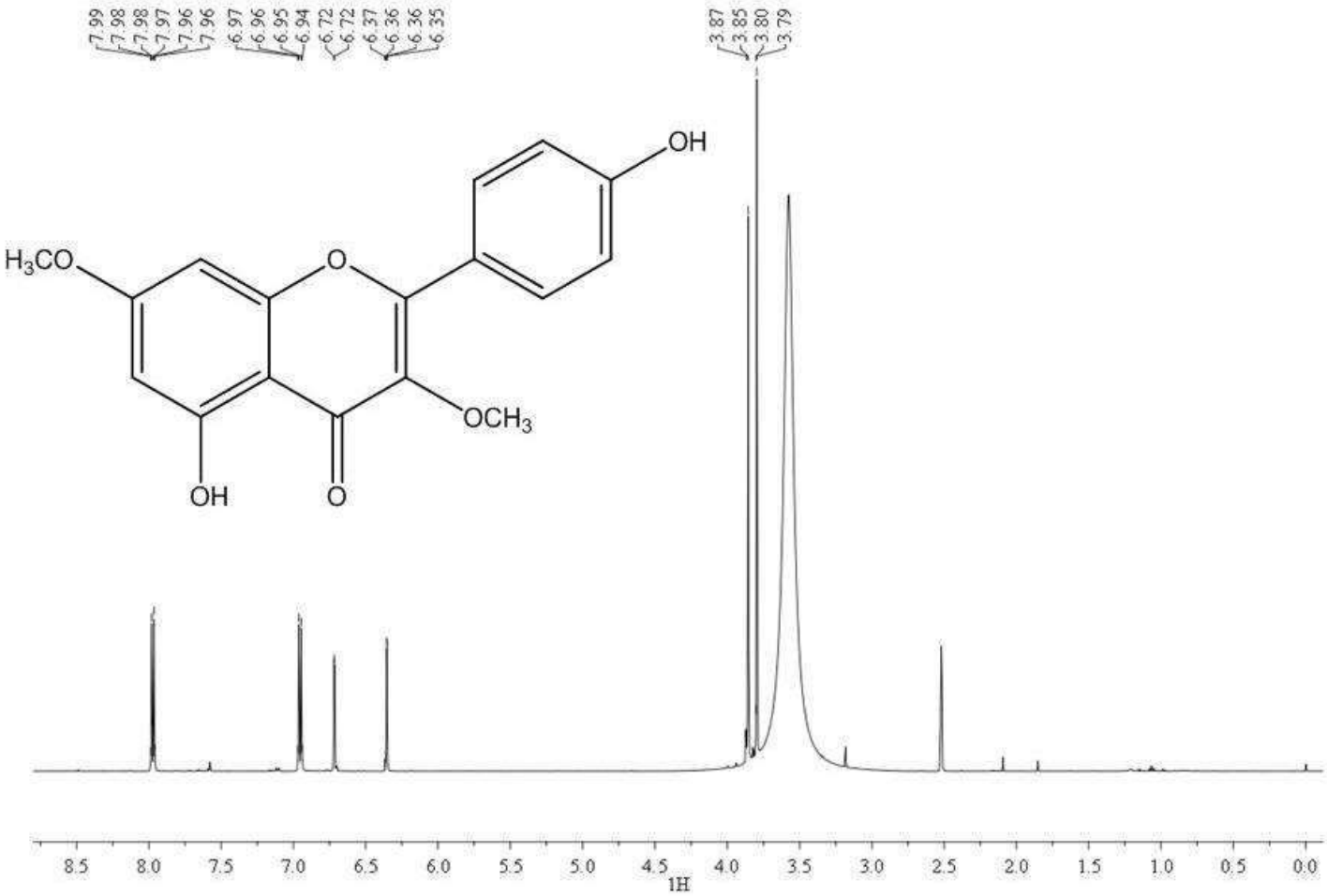

Fig. S45 ^{1}H NMR spectrum (DMSO-*d*6, 500 MHz) of 3,7-di-*O*-methyl-kaempferol (kumatakenin), **3** (**Fr-11B**).

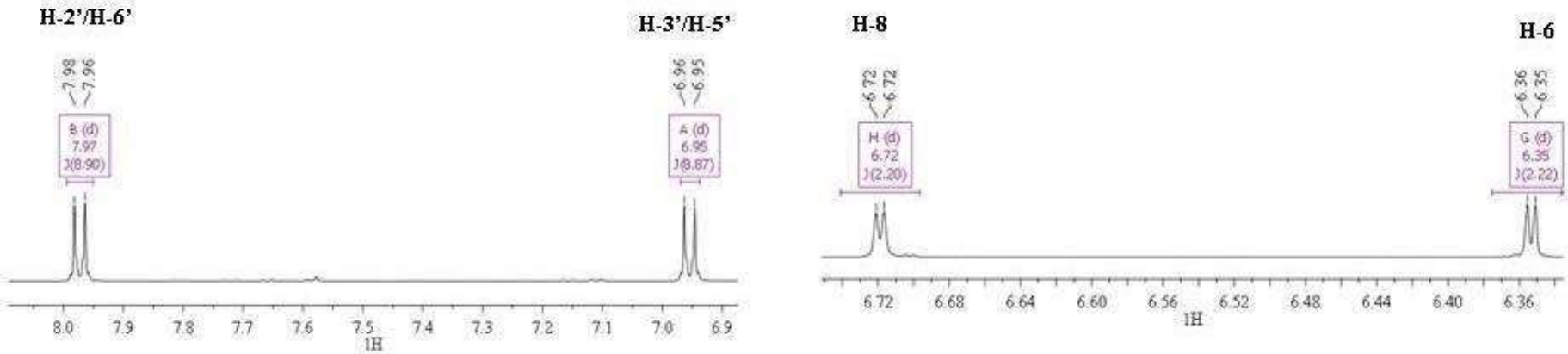

Fig. S46 ^{1}H NMR spectrum (DMSO-*d*6, 500 MHz) expanded in the aromatic protons region of 3,7-di-*O*-methyl-kaempferol (kumatakenin), **3** (**Fr-11B**).

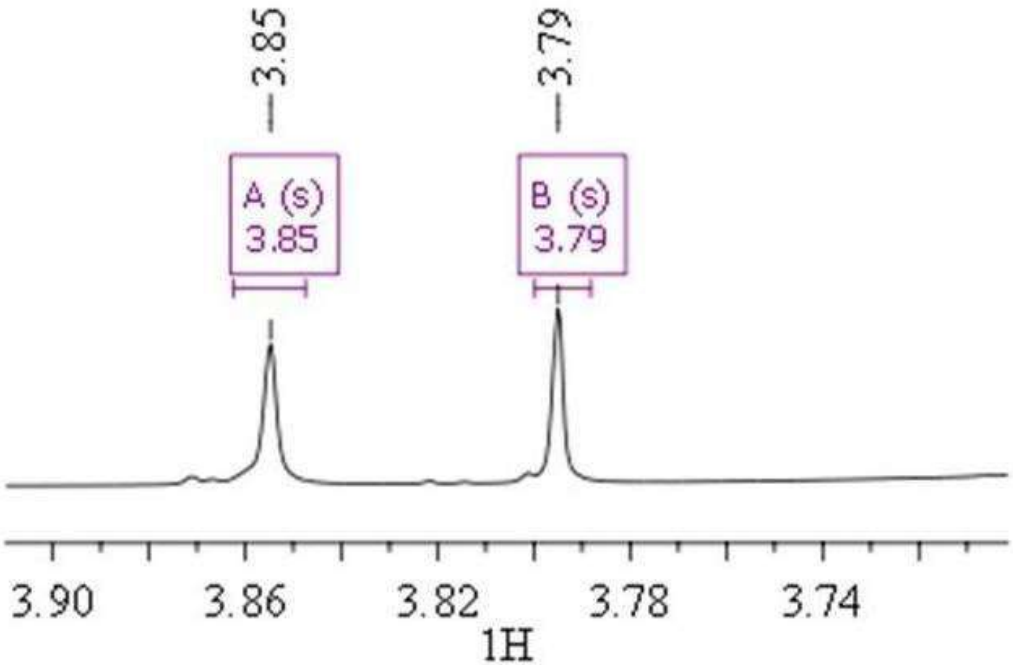

Fig. S47 ^{1}H NMR spectrum (DMSO-*d*6, 500 MHz) expanded in the region relative to methoxyl groups of 3,7-di-*O*-methyl-kaempferol (kumatakenin), **3** (**Fr-11B**).

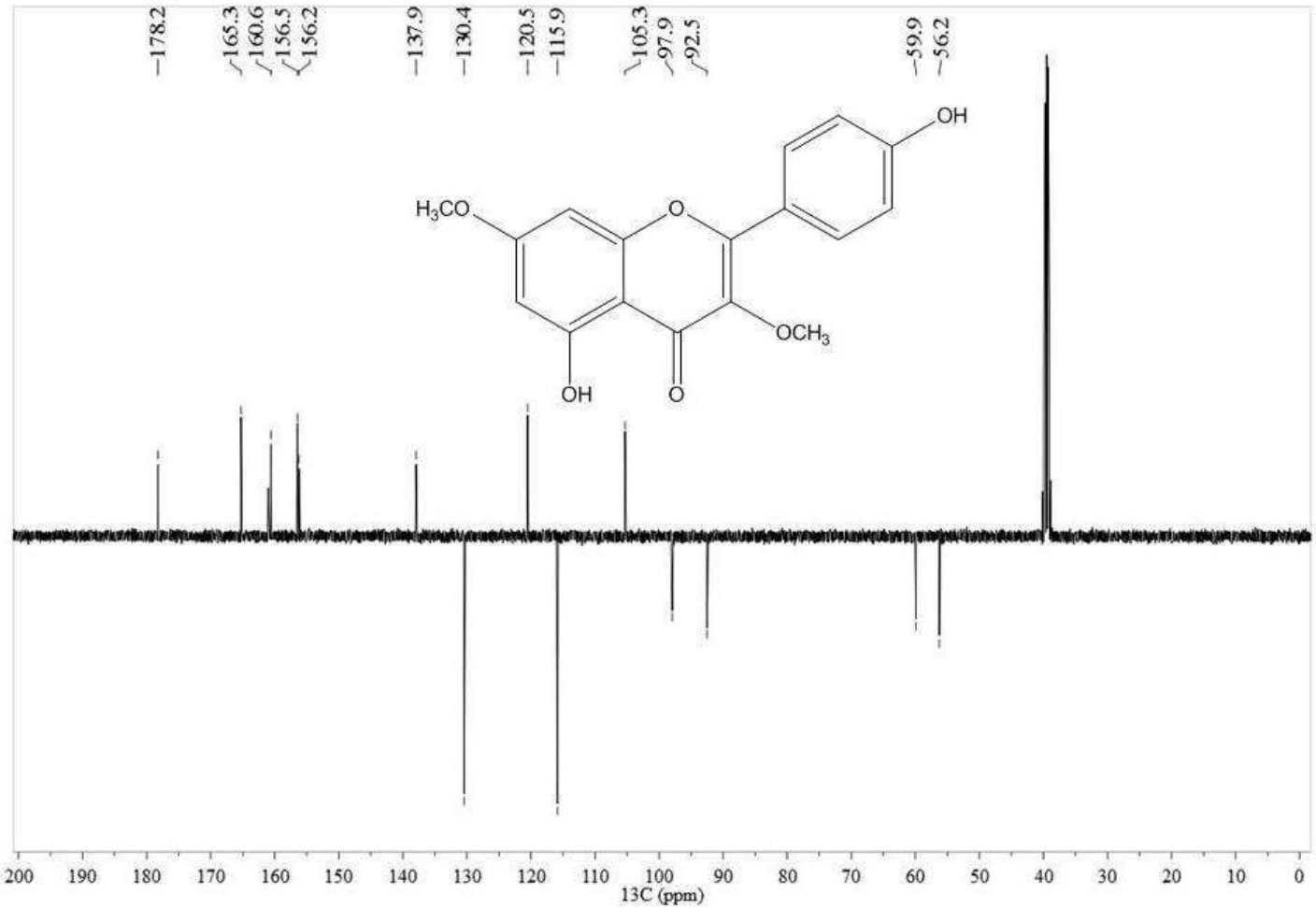

Fig. S48 APT NMR spectrum (DMSO-*d*6, 500 MHz) of 3,7-di-*O*-methyl-kaempferol (kumatakenin), **3** (**Fr-11B**).

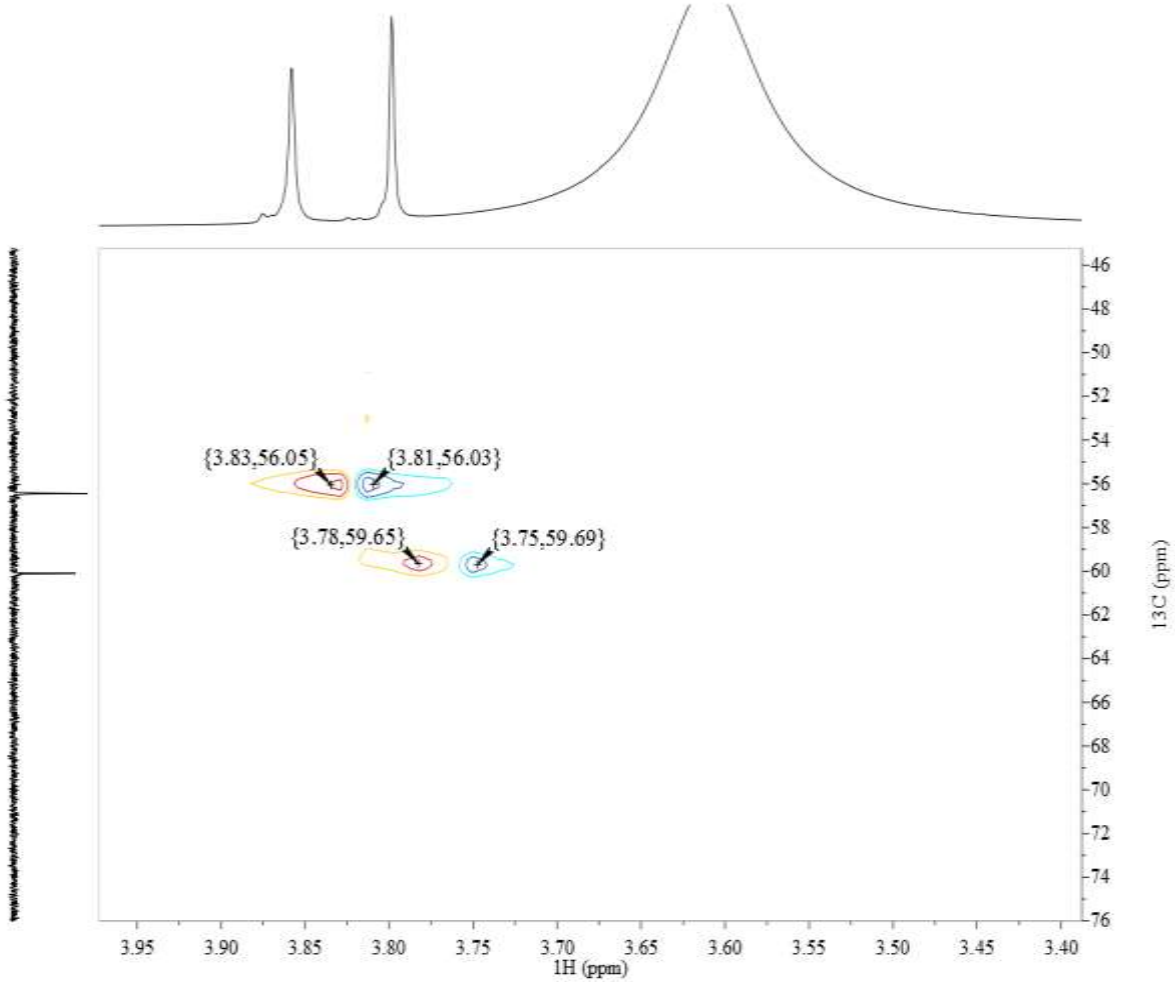

Fig. S49 HSQC ^{1}H-^{13}C NMR spectrum (DMSO-*d*6, 500 MHz) expanded in the region relative to methoxyl groups of 3,7-di-*O*-methyl-kaempferol (kumatakenin), **3** (**Fr-11B**).

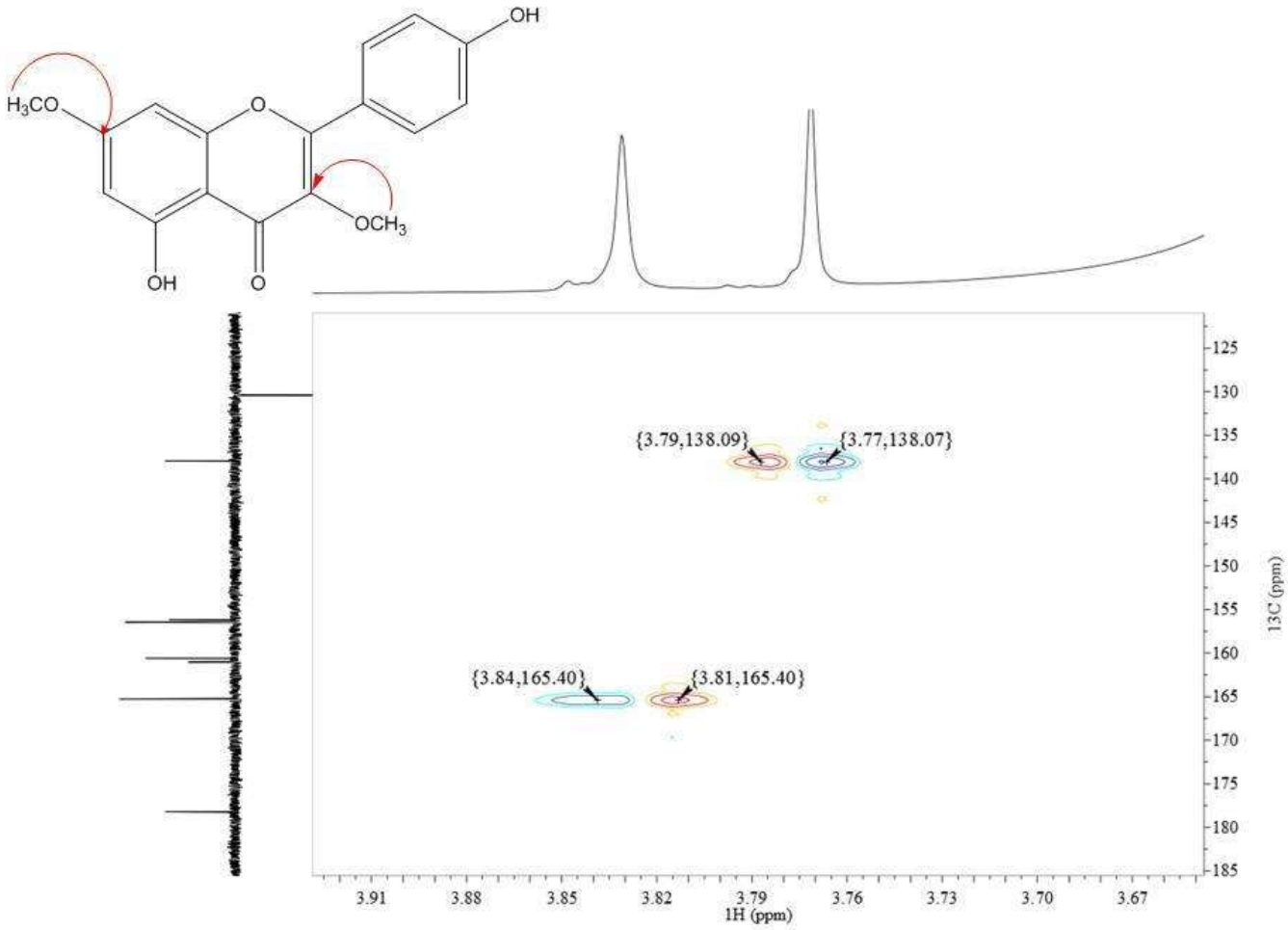

Fig. S50 HMBC ^{1}H-^{13}C NMR spectrum (DMSO-*d*6, 500 MHz) expanded in the region relative to the methoxyl groups of 3,7-di-*O*-methyl-kaempferol (kumatakenin), **3** (**Fr-11B**).

Table S3 Retention times and UV bands by HPLC-DAD and DI-APCI (+)-MS/MS for the annotated compounds.

ID	R_t(min) (%)*	UV (λ=280nm)	$[M+H]^+$ (intensity)	MS^2	Compounds Annotated
Fr-7 **(S2;S8;S9)**	29.4 (74.8%)	250; 355	345.2 (100%)	330 (- CH_3); 315 (- 2xCH_3)	3,3',4'-tri-*O*-methyl-quercetin, **1**
Fr-8 **(S3;S10;S11)**	32.2 (11.3%)	265; 350	315.2 (8%)	-	di-*O*-methyl-kaempferol
	32.7 (87.6%)	250; 350	345.2 (100%)	330 (- CH_3); 315 (- 2xCH_3)	tri-*O*-methyl-quercetin
Fr-9 **(S4;S12;S13)**	32.2 (69.4%)	255; 355	315.3 (64%)	300 (- CH_3); 287 (Aglycone)	di-*O*-methyl-kaempferol

	32.7 (30.1%)	265; 350	345.3 (100%)	330 (- CH_3); 312 (- CH_3-H_2O)	tri-*O*-methyl-quercetin
Fr-10 **(S5;S14;S15)**	32.2 (98.7%)	265; 345	315.2 (100%)	300 (- CH_3); 287 (Aglycone)	3,7-di-*O*-methyl-kaempferol (kumatakenin), **3**
Fr-11 **(S6;S16;S17)**	32.2 (79.3%)	265; 345	315.2 (100%)	300 (- CH_3); 287 (Aglycone)	3,7-di-*O*-methyl-kaempferol (kumatakenin), **3**
	36.7 (16.8%)	250; 350	359.3 (64%)	344 (- CH_3)	3,7,3',4'-tetra-*O*-methyl-quercetin (retusin), **2**
Fr-12 **(S7;S18;S19)**	32.2 (20.16%)	265; 345	315.2 (23%)	300 (- CH_3)	di -*O*-methyl-kaempferol
	36.7 (63.64%)	250; 350	359.3 (100%)	344 (-CH_3)	tetra-*O*-methyl-quercetin

*These percentages were taken from the area of the HPLC-UV chromatogram at 280 nm.

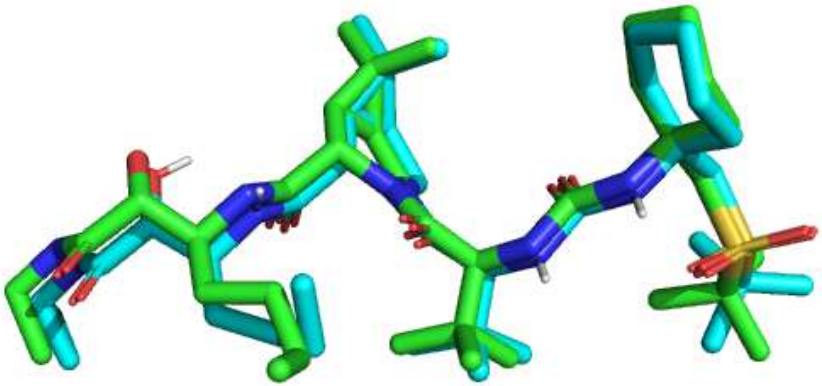

Fig. S51 Redocking result for 3CLpro crystal (PDBid: 6XQT). In green, the ligand Narlaprevir; in light cyan, pose 1 of the redocking result. Atoms: Dark blue - Nitrogen; Red - Oxygen. RMSD: 0.97 Å.

Table S4: Energy redocking values for 3CLpro with Narlaprevir, and PLpro interact with 5-amino-2-methyl-N-[(1R)-1-naphthalen-1-ylethyl]benzamide (GRL0617).

	3CLpro					PLpro		
	Affinity for best distance mode (kcal/mol)	Mode	Distance His41 (Å)	Distance Cys145 (Å)	Distance Glu166 (Å)	Affinity for best distance mode (kcal/mol)	Mode	Distance Tyr268 (Å)
Narlaprevir	-10,4	1	2,2	-	3,11	-	-	-
5-amino-2-methyl-N-[(1R)-1-naphthalen-1-ylethyl]benzamide (GRL0617)	-	-	-	-	-	-9,6	1	2,6

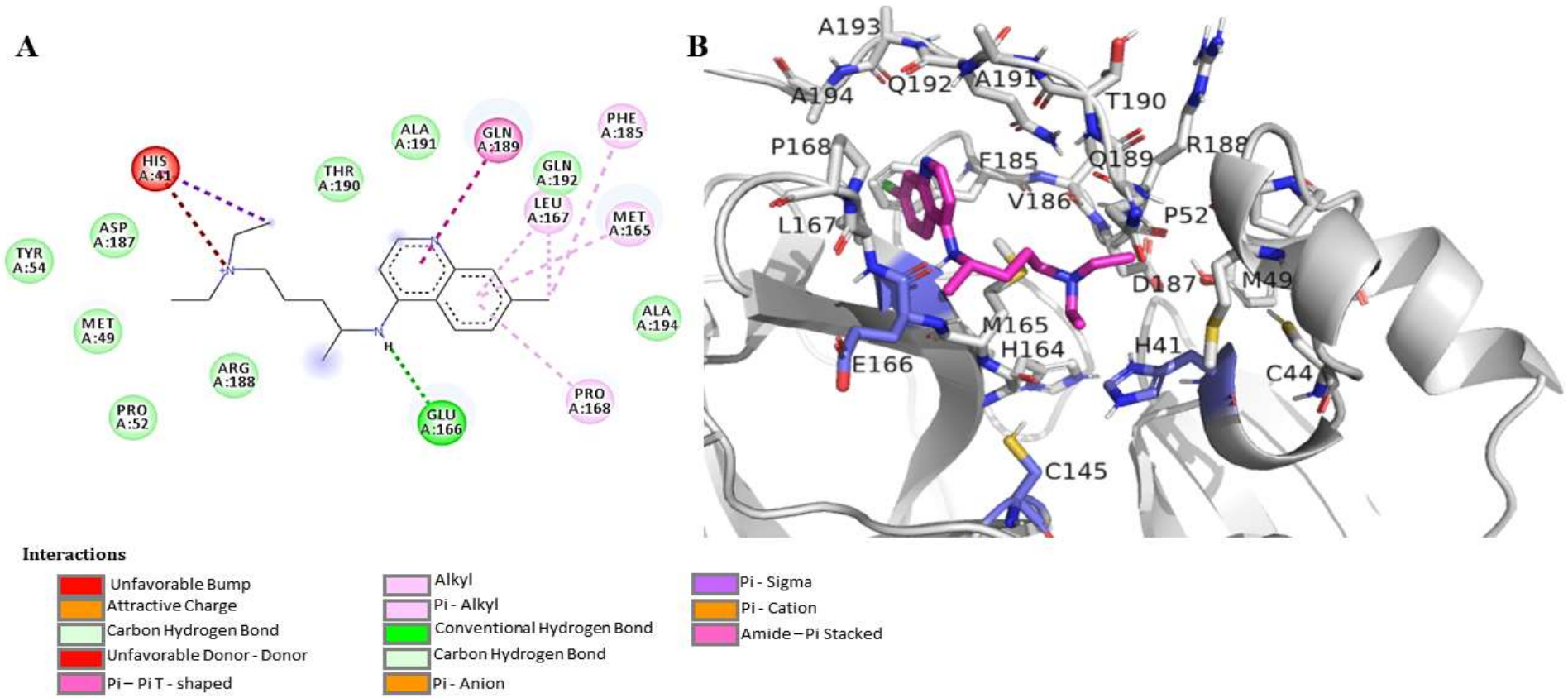

Fig. S52 Interaction map of the amino acid residues of the 3CLpro (PDBid: 6XQT) with chloroquine. Figure **A** shows the different types of interaction between the protein and the ligand in flat representation. The 3D representation is in Figure **B**, in which the 3CLpro is in gray and residues within a radius of proximity equal to 5Å of the ligand, represented by sticks, and the ligand is in magenta. In lavender are the residues His41, Cys145 and Glu166.

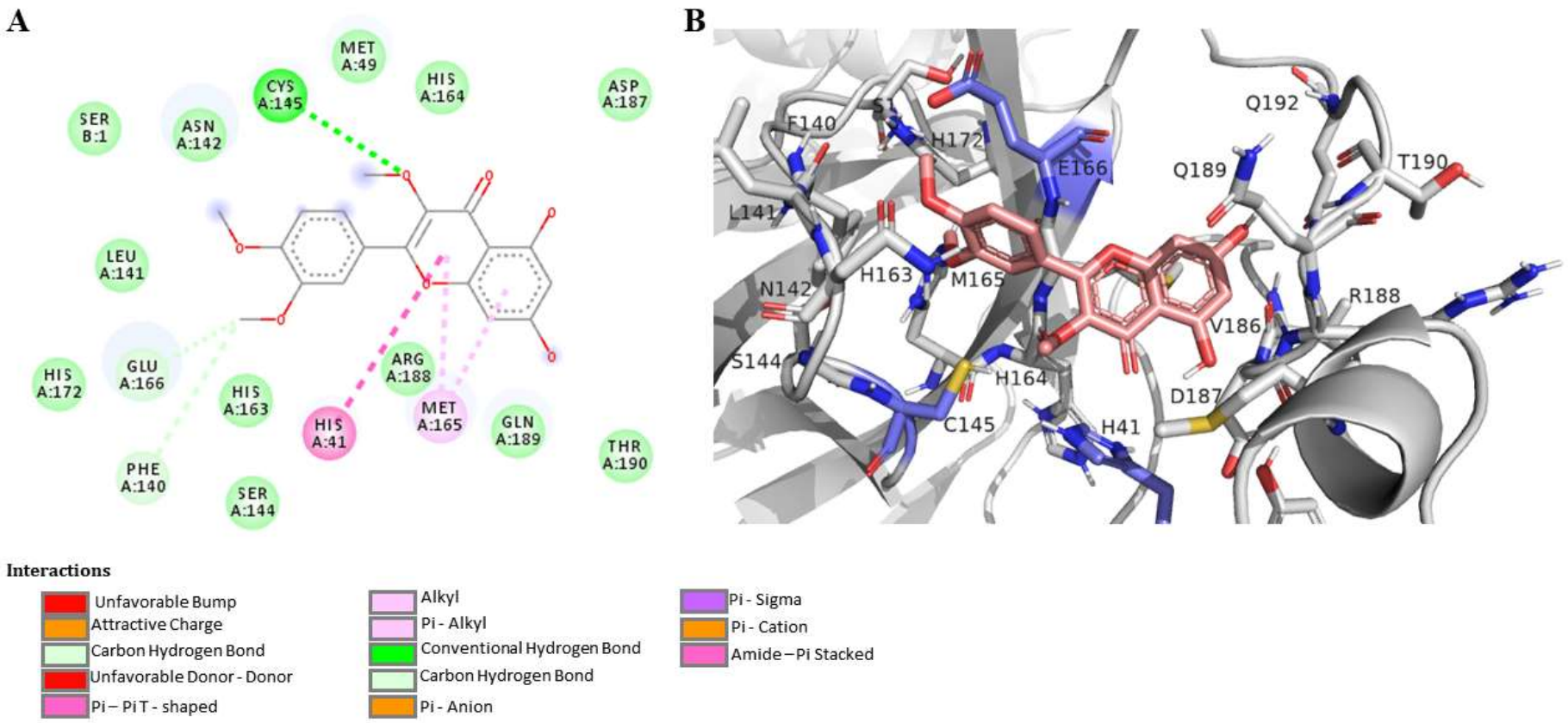

Fig.S53 Interaction map of the amino acid residues of the 3CLpro (PDBid: 6XQT) with 3,3 ',4'-tri-*O*-methyl-quercetin **(1).** Figure **A** shows the different types of interaction between the protein and the ligand in flat representation. The 3D representation is in Figure **B**, in which the 3CLpro is in gray and residues within a radius of proximity equal to 5Å of the ligand, represented by sticks, and the ligand is in light pink. In lavender are the residues His41, Cys145 and Glu166.

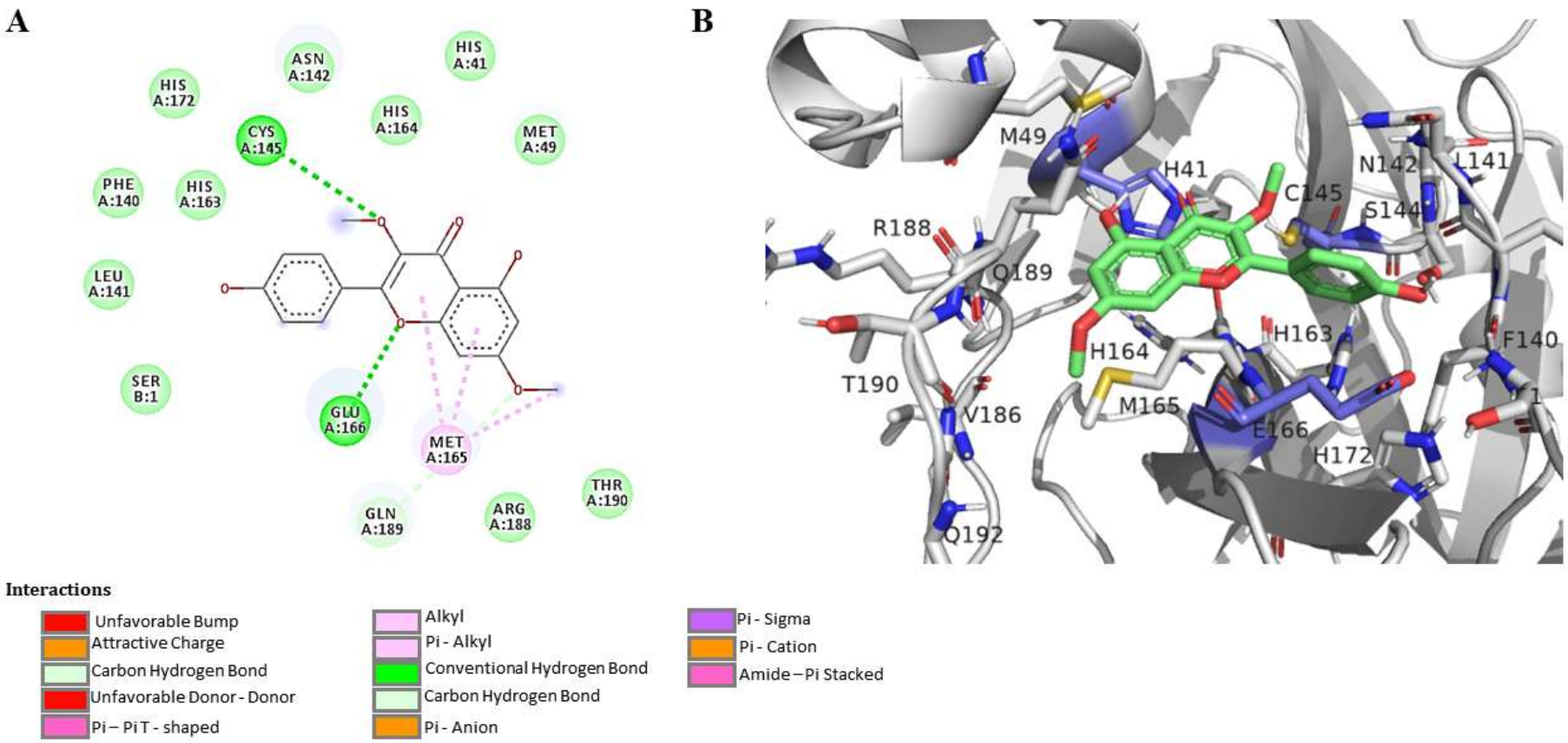

Fig.S54 Interaction map of the amino acid residues of the 3CLpro (PDBid: 6XQT) with 3,7-di-*O*-methyl-kaempferol (kumatakenin) **(3).** Figure **A** shows the different types of interaction between the protein and the ligand in flat representation. The 3D representation is in Figure **B**, in which the 3CLpro is in gray and residues within a radius of proximity equal to 5Å of the ligand, represented by sticks, and the ligand is in green. In lavender are the residues His41, Cys145 and Glu166.

Fig. S55 Redocking result for PLpro crystal (PDBid: 7JRN). In gold, the ligand 5-amino-2-methyl-N - [(1R) -1-naphthalen-1-ylethyl] benzamide (GRL0617); in light blue, pose 1 of the redocking result. Atoms: Dark blue - Nitrogen; White - Hydrogen; Red: Oxygen. RMSD: 0.45356 Å

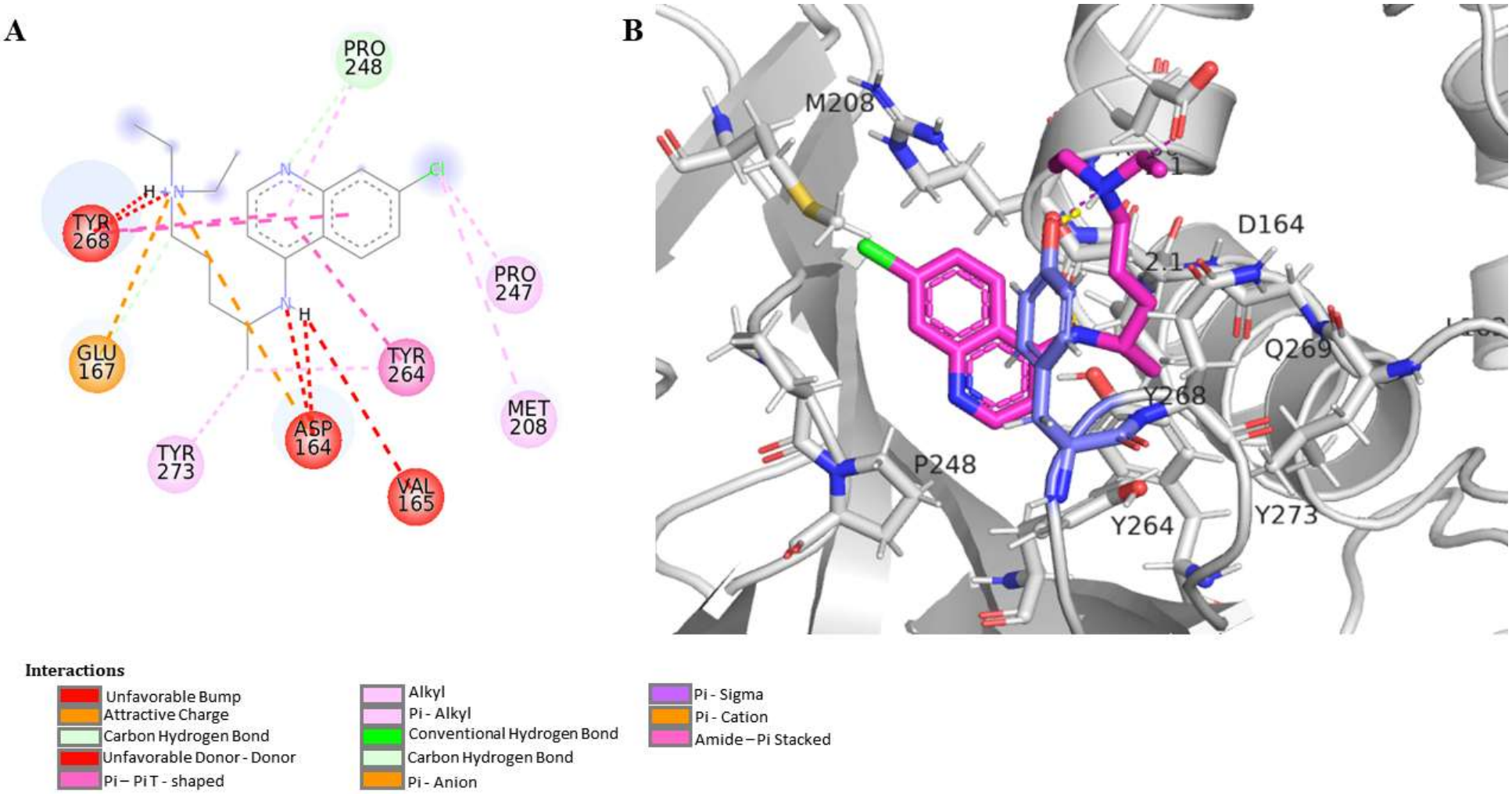

Fig. S56 Interaction map of the amino acid residues of the PLpro (PDBid: 7JRN) with chloroquine**.** Figure **A** shows the different types of interaction between the protein and the ligand in flat representation. The 3D representation is in Figure **B**, in which the PLpro is in gray and residues within a radius of proximity equal to 5Å of the ligand, represented by sticks, and the ligand is in magenta. In lavender the residue Tyr268.

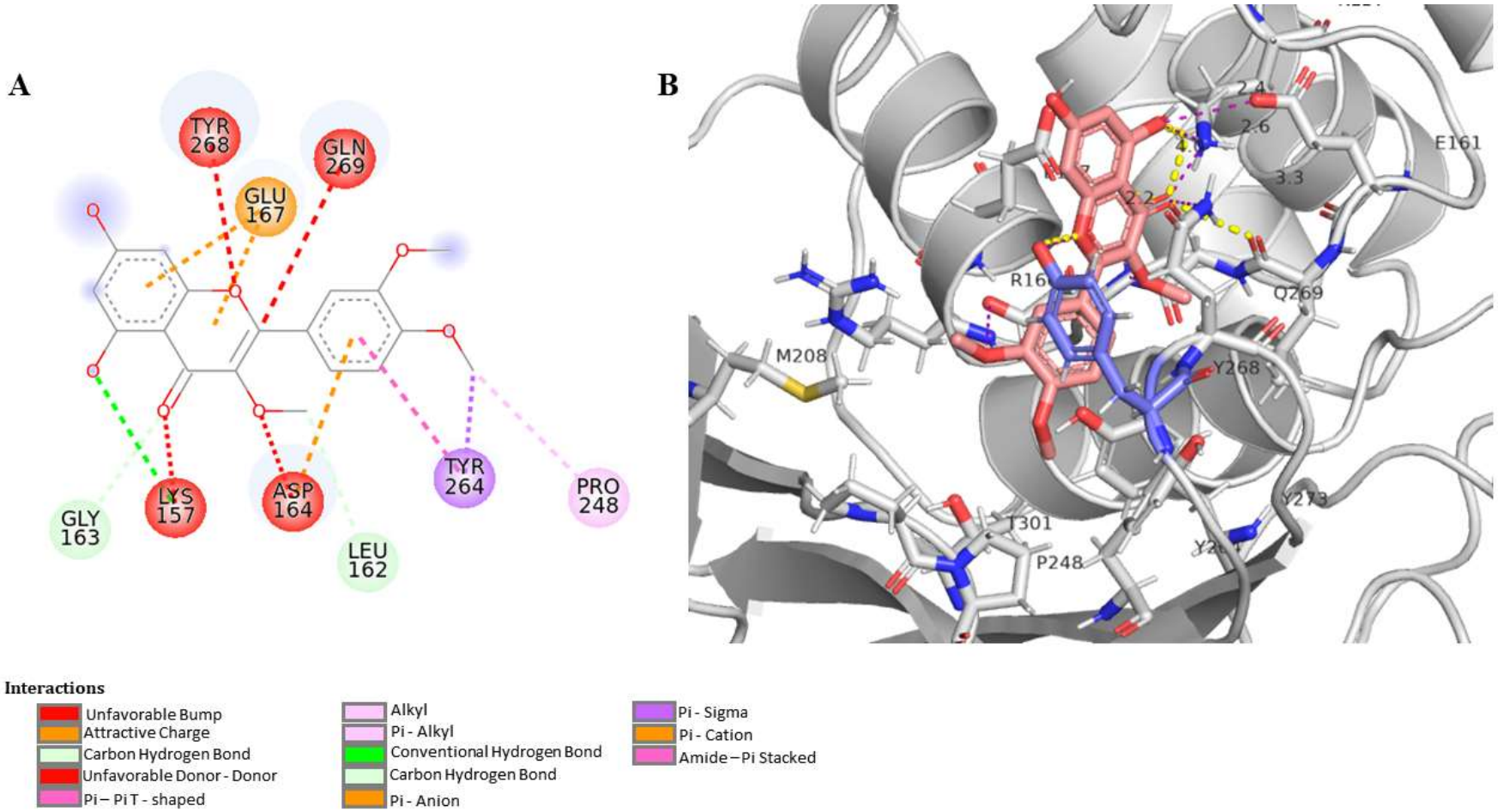

Fig. S57 Interaction map of the amino acid residues of the PLpro (PDBid: 7JRN) with 3,3 ',4'-tri-*O*-methyl-quercetin **(1).** Figure **A** shows the different types of interaction between the protein and the ligand in flat representation. The 3D representation is in Figure **B**, in which the PLpro is in gray and residues within a radius of proximity equal to 5Å of the ligand, represented by sticks, and the ligand is in light pink. In lavender the residue Tyr268.

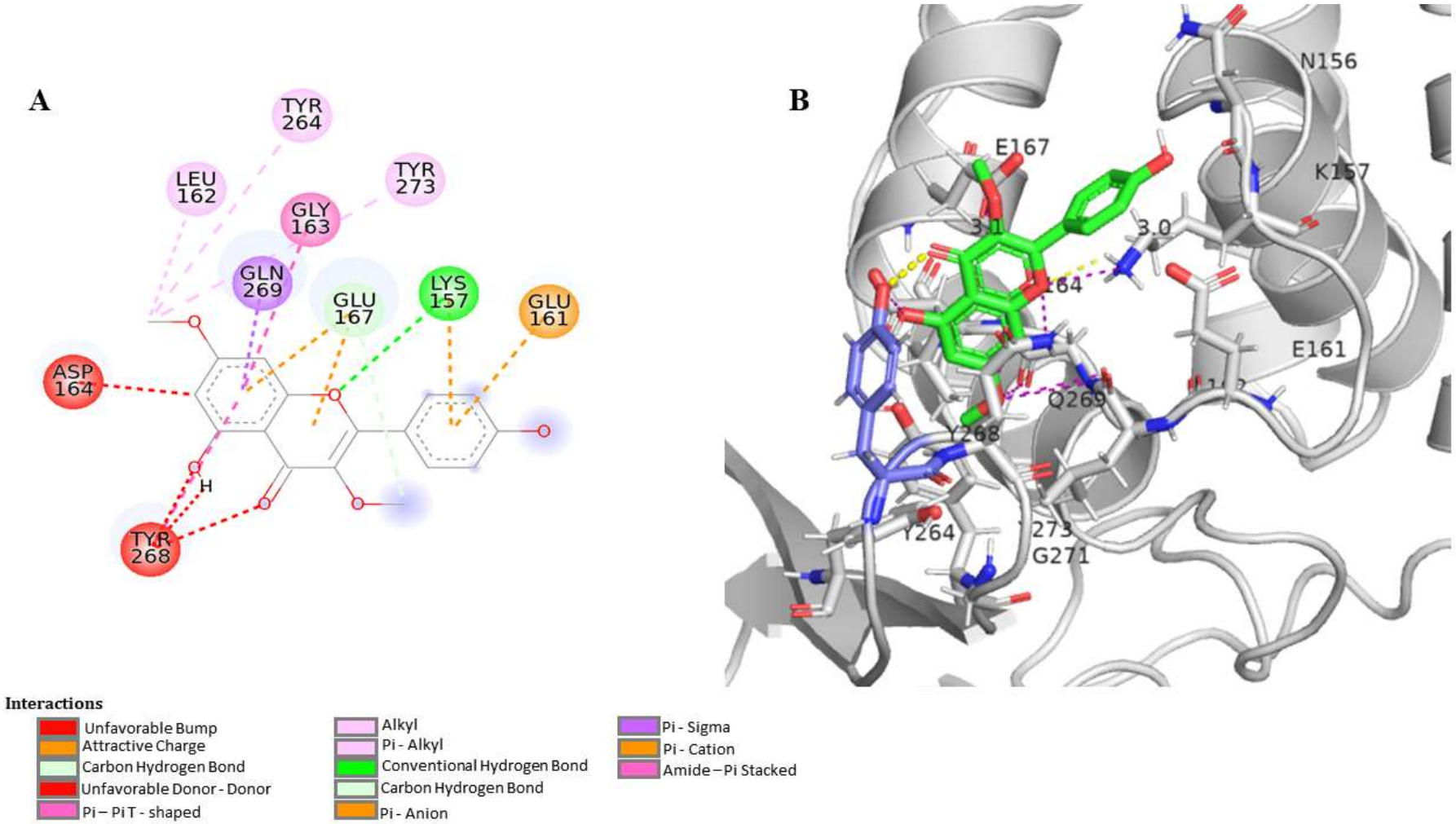

Fig. S58 Interaction map of the amino acid residues of the PLpro (PDBid: 7JRN) with 3,7-di-*O*-methyl-kaempferol (kumatakenin) **(3).** Figure **A** shows the different types of interaction between the protein and the ligand in flat representation. The 3D representation is in Figure **B**, in which the PLpro is in gray and residues within a radius of proximity equal to 5Å of the ligand, represented by sticks, and the ligand is in green. In lavender the residue Tyr268.